

profile of TCP-CCPs was further compared with a commercially available transfection reagent, ExGen 500 (linear polyethyleneimine (LPEI)). Compared to TCP-CCPs, LPEI polyplexes prepared at [amine]/[phosphate] (N/P) = 6, according to the manufacturer's protocol, allowed much higher transfection efficiency (Supporting Information, Figure 3), but also induced higher cytotoxicity (Supporting Information, Figure 4). On the other hand, TCP-CCPs achieved higher transfection efficiency with lower cytotoxicity compared to LPEI polyplexes prepared at N/P = 2, close to the charge-neutralized point between LPEI and pDNA. Altogether, the TCP-CCPs demonstrated enhanced transfection efficiency with decreased cytotoxicity.

3.6. Intracellular Trafficking of Polyplex Formulations.

Successful gene transfection in the GLuc assay encouraged us to further investigate the intracellular trafficking of the TCP-CCPs to elucidate the mechanism of enhanced transfection efficiency. Thus, the intracellular trafficking (specifically, the endosomal escape) of each polyplex (BPs, BCPs, TCP-CCPs, and TCP-nCCPs) incorporating Cy5-labeled pDNA was observed with CLSM after 24, 48, and 72 h incubation with Huh-7 cells. In the CLSM images, pDNA entrapped by the late endosome/lysosome appears yellow due to a combination of the Cy5-labeled pDNA signal (red) overlapping with the late endosome/lysosome signals (green) stained with LysoTracker Green. Successful release of pDNA from the late endosomes/lysosomes results in an increase of red pixels (or a decrease of yellow pixels) in the CLSM image. The number of red pixels clearly increased after 48 h incubation with TCP-CCPs, compared to the other polyplexes (Figure 6a–d), suggesting that a substantial portion of Cy5-labeled pDNA was delivered into the cytoplasm. Note that a large fraction of the red signals were shown as a punctate pattern, similar to the previously reported CLSM images observed for nanoparticles featuring the endosomal escaping functionality.^{38–44} The punctate pattern might be due to substantially small diffusion coefficients of the polyplexes carrying pDNA (or uncomplexed pDNAs) in the cytoplasm.^{45,46} The endosomal escape efficiency of each polyplex was then quantified based on the colocalization ratio of Cy5-labeled pDNA signals with the late endosome/lysosome signals in each CLSM image (Figure 6a–d and Supporting Information, Figure 5). This analysis showed that TCP-CCPs exhibited significantly lower colocalization ratios of pDNA with the late endosome/lysosome, compared to the other polyplexes (Figure 6e), indicating that the most effective endosomal escape was achieved by coating BCPs with PEG-CCP. Note that TCP-nCCPs exhibited significantly higher colocalization ratios than the template BCPs, suggesting that coating BCPs with PEG-nCCP compromised their endosomal escape. This compromised endosomal escape could be explained by the fact that TCP-nCCPs lacking acidic pH-sensitivity were equipped with stable PEG palisades in the acidic conditions (Figure 2b), rendering the positively charged template BCPs less active for the endosomal membrane. The obtained colocalization ratios (Figure 6e) were well-correlated with the transfection efficiency (Figure 4), indicating that the enhanced transfection efficiency of TCP-CCPs was most likely due to the endosomal escape facilitated by the charge-conversional property of PAsp(DET-Aco) segment.

4. CONCLUSIONS

The present study was aimed to develop a smart gene carrier, that is, a biological environment-responsive TCP-CCP

formulation, featuring reversible stability, endosomal escaping functionality, and also high biocompatibility based on pH/disulfide reduction dual intracellular environment-responsive chemistries. The obtained results demonstrated that reversible stability was achieved by disulfide cross-linking of polyplexes and endosomal escaping functionality was provided by coating polyplexes with acidic pH-sensitive PEG-CCP. Ultimately, the TCP-CCP appreciably enhanced gene transfection efficiency without associated cytotoxicity. The TCP-CCP formulation described here represents a fundamental step toward development of synthetic gene vectors that can mimic the multifunctional abilities of their natural viral counterparts. The fundamental improvements in gene carrier performance open the door to further improvements for enhanced site-specific accumulation and cell uptake of polyplexes by presentation of bioactive moieties (e.g., cyclic RGD^{34,47,48}) on their surface.

■ ASSOCIATED CONTENT

Ⓢ Supporting Information

¹H NMR spectrum of thiolated PLys, size distribution (intensity) histograms of polyplexes, transfection study in comparison with a commercially available transfection reagent ExGen 500, cytotoxicity study in comparison with ExGen 500, and CLSM images showing intracellular distribution of polyplexes (or Cy5-labeled pDNA) at varying incubation times are represented in Supporting Figures 1, 2, 3, 4, and 5, respectively. This material is available free of charge via the Internet at <http://pubs.acs.org>.

■ AUTHOR INFORMATION

Corresponding Author

*Tel: +81-3-5841-7138 (K.K.); +81-3-5841-1701 (K.M.). Fax: +81-3-5841-7139 (K.K.); +81-3-5841-7139 (K.M.). E-mail: kataoka@bmw.t.u-tokyo.ac.jp (K.K.); miyata@bmw.t.u-tokyo.ac.jp (K.M.).

Notes

The authors declare no competing financial interest.

■ ACKNOWLEDGMENTS

This research was financially supported by the Funding Program for World-Leading Innovative R&D in Science and Technology (FIRST), the Japan Society for the Promotion of Science (JSPS), and the Core Research Program for Evolutional Science and Technology (CREST) from the Japan Science and Technology Agency (JST).

■ ABBREVIATIONS

| | |
|----------|---|
| BP | binary non-cross-linked polyplex (pDNA/PLys) |
| TP | ternary non-cross-linked polyplex |
| TP-CCP | BP coated with PEG-CCP (pDNA/PLys/PEG-CCP) |
| TP-nCCP | BP coated with PEG-nCCP (pDNA/PLys/PEG-nCCP) |
| BCP | binary cross-linked polyplex (pDNA/thiolated PLys) |
| TCP | ternary cross-linked polyplex |
| TCP-CCP | BCP coated with PEG-CCP (pDNA/thiolated PLys/PEG-CCP) |
| TCP-nCCP | BCP coated with PEG-nCCP (pDNA/thiolated PLys/PEG-nCCP) |

REFERENCES

- (1) Kabanov, A. V.; Kabanov, V. A. *Bioconjugate Chem.* **1995**, *6*, 7–20.
- (2) Kakizawa, Y.; Kataoka, K. *Adv. Drug Delivery Rev.* **2002**, *54*, 203–222.
- (3) Pack, D. W.; Hoffman, A. S.; Pun, S.; Stayton, P. S. *Nat. Rev. Drug Discovery* **2005**, *4*, 581–593.
- (4) Neu, M.; Fischer, D.; Kissel, T. *J. Gene Med.* **2005**, *7*, 992–1009.
- (5) Luten, J.; van Nostrum, C. F.; Smedt, S. C. D.; Hennink, W. E. *J. Controlled Release* **2008**, *126*, 97–110.
- (6) Miyata, K.; Nishiyama, N.; Kataoka, K. *Chem. Soc. Rev.* **2012**, *41*, 2562–2574.
- (7) Wagner, E. *Acc. Chem. Res.* **2012**, *45*, 1005–1013.
- (8) Pillay, C. S.; Elliott, E.; Dennison, C. *Biochem. J.* **2002**, *363*, 417–429.
- (9) Saito, G.; Swanson, J. A.; Lee, K. D. *Adv. Drug Delivery Rev.* **2003**, *55*, 199–215.
- (10) Kim, Y. H.; Park, J. H.; Lee, M.; Kim, Y.-H.; Park, T. G.; Kim, S. W. *J. Controlled Release* **2005**, *103*, 209–219.
- (11) Walker, G. F.; Fella, C.; Pelisek, J.; Fahrmeir, J.; Boeckle, S.; Ogris, M.; Wagner, E. *Mol. Ther.* **2005**, *11*, 418–425.
- (12) Knorr, V.; Russ, V.; Allmendinger, L.; Ogris, M.; Wagner, E. *Bioconjugate Chem.* **2008**, *19*, 1625–1634.
- (13) Rozema, D. B.; Ekena, K.; Lewis, D. L.; Loomis, A. G.; Wolff, J. A. *Bioconjugate Chem.* **2003**, *14*, 51–57.
- (14) Lee, Y.; Miyata, K.; Oba, M.; Ishii, T.; Fukushima, S.; Han, M.; Koyama, H.; Nishiyama, N.; Kataoka, K. *Angew. Chem., Int. Ed.* **2008**, *47*, 5163–5166.
- (15) Sanjoh, H.; Hiki, H.; Lee, Y.; Oba, M.; Miyata, K.; Ishii, T.; Kataoka, K. *Macromol. Rapid Commun.* **2010**, *31*, 1181–1186.
- (16) Kakizawa, Y.; Harada, A.; Kataoka, K. *J. Am. Chem. Soc.* **1999**, *121*, 11247–11248.
- (17) Trubetskoy, V. S.; Loomis, A.; Slattum, P. M.; Hagstrom, J. E.; Budker, V. G.; Wolff, J. A. *Bioconjugate Chem.* **1999**, *10*, 624–628.
- (18) Kwok, K. Y.; McKenzie, D. L.; Evers, D. L.; Rice, K. G. *J. Pharm. Sci.* **1999**, *88*, 996–1003.
- (19) Kakizawa, Y.; Harada, A.; Kataoka, K. *Biomacromolecules* **2001**, *2*, 491–497.
- (20) Oupicky, D.; Carlisle, R. C.; Seymour, L. W. *Gene Ther.* **2001**, *8*, 713–724.
- (21) Gosselin, M. A.; Guo, W. J.; Lee, R. J. *Bioconjugate Chem.* **2001**, *12*, 989–994.
- (22) Oupicky, D.; Parker, A. L.; Seymour, L. W. *J. Am. Chem. Soc.* **2002**, *124*, 8–9.
- (23) Miyata, K.; Kakizawa, Y.; Nishiyama, N.; Harada, A.; Yamasaki, Y.; Koyama, H.; Kataoka, K. *J. Am. Chem. Soc.* **2004**, *126*, 2355–2361.
- (24) Takae, S.; Miyata, K.; Oba, M.; Ishii, T.; Nishiyama, N.; Itaka, K.; Yamasaki, Y.; Koyama, H.; Kataoka, K. *J. Am. Chem. Soc.* **2008**, *130*, 6001–6009.
- (25) Trubetskoy, V. S.; Loomis, A.; Hagstrom, J. E.; Budker, V. G.; Wolff, J. A. *Nucleic Acids Res.* **1999**, *27*, 3090–3095.
- (26) Trubetskoy, V. S.; Wong, S. C.; Subbotin, V.; Budker, V. G.; Loomis, A.; Hagstrom, J. E.; Wolff, J. A. *Gene Ther.* **2003**, *10*, 261–271.
- (27) Ito, T.; Iida-Tanaka, N.; Niidome, T.; Kawano, T.; Kubo, K.; Yoshikawa, K.; Sato, T.; Yang, Z. H.; Koyama, T. *J. Controlled Release* **2006**, *112*, 382–388.
- (28) Miyata, K.; Oba, M.; Nakanishi, M.; Fukushima, S.; Yamasaki, Y.; Koyama, H.; Nishiyama, N.; Kataoka, K. *J. Am. Chem. Soc.* **2008**, *130*, 16287–16294.
- (29) Uchida, H.; Miyata, K.; Oba, M.; Ishii, T.; Suma, T.; Itaka, K.; Nishiyama, N.; Kataoka, K. *J. Am. Chem. Soc.* **2011**, *133*, 15524–15532.
- (30) Pittella, F.; Zhang, M.; Lee, Y.; Kim, H.-J.; Tockary, T.; Osada, K.; Ishii, T.; Miyata, K.; Nishiyama, N.; Kataoka, K. *Biomaterials* **2011**, *32*, 3106–3114.
- (31) Pittella, F.; Miyata, K.; Maeda, Y.; Suma, T.; Chen, Q.; Christie, R. J.; Osada, K.; Nishiyama, N.; Kataoka, K. *J. Controlled Release* **2012**, *161*, 868–874.
- (32) Harada, A.; Cammas, S.; Kataoka, K. *Macromolecules* **1996**, *29*, 6183–6188.
- (33) Oba, M.; Vachutinsky, Y.; Miyata, K.; Kano, M. R.; Ikeda, S.; Nishiyama, N.; Itaka, K.; Miyazono, K.; Koyama, H.; Kataoka, K. *Mol. Pharm.* **2010**, *7*, 501–509.
- (34) Vachutinsky, Y.; Oba, M.; Miyata, K.; Hiki, S.; Kano, M. R.; Nishiyama, N.; Koyama, H.; Miyazono, K.; Kataoka, K. *J. Controlled Release* **2011**, *149*, 51–57.
- (35) Boeckle, S.; von Gersdorff, K.; van der Piepen, S.; Culmsee, C.; Wagner, E.; Ogris, M. *J. Gene Med.* **2004**, *6*, 1102–1111.
- (36) Uchida, S.; Itaka, K.; Chen, Q.; Osada, K.; Miyata, K.; Ishii, T.; Harada-Shiba, M.; Kataoka, K. *J. Controlled Release* **2011**, *155*, 296–302.
- (37) Nomoto, T.; Matsumoto, Y.; Miyata, K.; Oba, M.; Fukushima, S.; Nishiyama, N.; Yamasoba, T.; Kataoka, K. *J. Controlled Release* **2011**, *151*, 104–109.
- (38) El-Sayed, A.; Khalil, I. A.; Kogure, K.; Futaki, S.; Harashima, H. *J. Biol. Chem.* **2008**, *283*, 23450–23461.
- (39) Kaneshiro, T. L.; Lu, Z.-R. *Biomaterials* **2009**, *30*, 5660–5666.
- (40) Xiong, X.-B.; Uludag, H.; Lavasanifar, A. *Biomaterials* **2010**, *31*, 5886–5893.
- (41) Takemoto, H.; Ishii, A.; Miyata, K.; Nakanishi, M.; Oba, M.; Ishii, T.; Yamasaki, Y.; Nishiyama, N.; Kataoka, K. *Biomaterials* **2010**, *31*, 8097–8105.
- (42) Guo, S.; Huang, Y.; Jiang, Q.; Sun, Y.; Deng, L.; Liang, Z.; Du, Q.; Xing, J.; Zhao, Y.; Wang, P. C.; Dong, A.; Liang, X.-J. *ACS Nano* **2010**, *4*, 5505–5511.
- (43) Yang, X.-Z.; Dou, S.; Wang, Y.-C.; Long, H.-Y.; Xiong, M.-H.; Mao, C.-Q.; Yao, Y.-D.; Wang, J. *ACS Nano* **2012**, *6*, 4955–4965.
- (44) Suma, T.; Miyata, K.; Anraku, Y.; Watanabe, S.; Christie, R. J.; Takemoto, H.; Shioyama, M.; Gouda, N.; Ishii, T.; Nishiyama, N.; Kataoka, K. *ACS Nano* **2012**, *6*, 6693–6705.
- (45) Lukacs, G. L.; Haggie, P.; Seksek, O.; Lechardeur, D.; Freedman, N.; Verkman, A. S. *J. Biol. Chem.* **2000**, *275*, 1625–1629.
- (46) Bausinger, R.; von Gersdorff, K.; Braeckmans, K.; Ogris, M.; Wagner, E.; Brauchle, C.; Zumbusch, A. *Angew. Chem., Int. Ed.* **2006**, *45*, 1568–1572.
- (47) Oba, M.; Fukushima, S.; Kanayama, N.; Aoyagi, K.; Nishiyama, N.; Koyama, H.; Kataoka, K. *Bioconjugate Chem.* **2007**, *18*, 1415–1423.
- (48) Kagaya, H.; Oba, M.; Miura, Y.; Koyama, H.; Ishii, T.; Shimada, T.; Takato, T.; Kataoka, T.; Miyata, T. *Gene Ther.* **2012**, *19*, 61–69.

Smart Multilayered Assembly for Biocompatible siRNA Delivery Featuring Dissolvable Silica, Endosome-Disrupting Polycation, and Detachable PEG

Tomoya Suma,[†] Kanjiro Miyata,^{*,†} Yasutaka Anraku,[‡] Sumiyo Watanabe,[†] R. James Christie,[†] Hiroyasu Takemoto,[§] Momoko Shioyama,[§] Noha Gouda,[†] Takehiko Ishii,[†] Nobuhiro Nishiyama,[†] and Kazunori Kataoka^{†,*,§,L,*}

[†]Department of Bioengineering, Graduate School of Engineering, The University of Tokyo, 7-3-1 Hongo, Bunkyo-ku, Tokyo 113-8656, Japan, [‡]Center for Disease Biology and Integrative Medicine, Graduate School of Medicine, The University of Tokyo, 7-3-1 Hongo, Bunkyo-ku, Tokyo 113-0033, Japan, [§]Department of Materials Engineering, Graduate School of Engineering, The University of Tokyo, 7-3-1 Hongo, Bunkyo-ku, Tokyo 113-8656, Japan, and ^LCenter for NanoBio Integration, The University of Tokyo, 7-3-1 Hongo, Bunkyo-ku, Tokyo 113-8656, Japan

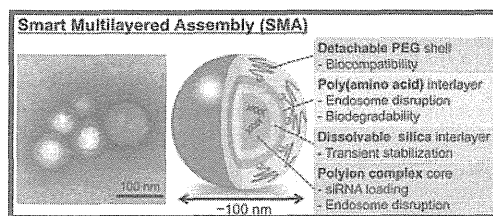
Small interfering RNA (siRNA) has generated tremendous research interest in therapeutic applications for the treatment of various intractable diseases caused by aberrant gene expression, such as cancer.^{1,2} This interest stems from the highly specific and potent gene silencing ability inherent to siRNA, termed RNA interference (RNAi). In order to attain therapeutic benefit, siRNA needs to overcome several biological hurdles, such as rapid renal clearance, enzymatic decomposition, distribution in nontarget tissues, inefficient cellular uptake, and endosomal/lysosomal entrapment. To date, various types of nanoparticle formulations have been developed as a delivery vehicle of siRNA, *e.g.*, polymer-based complexes (polyplexes),^{3–12} lipid-based complexes (lipoplexes),^{13–15} silica nanoparticles,^{16,17} calcium phosphate nanoparticles,^{18,19} gold nanoparticles,^{20,21} and also their hybrid systems. Nevertheless, further improvement of siRNA vehicles is still demanded to gain better therapeutic efficacy for their translation into pharmaceutical agents.

Several properties required for the ideal siRNA vehicle are apparently conflicting, *i.e.*, high stability for siRNA protection in extracellular conditions vs smooth payload release within the cytoplasm and reduced nonspecific interactions with biomacromolecules (or biocompatibility) vs efficient cellular uptake (endocytosis) and subsequent endosomal escape in target cells. One promising solution to these conflicts is to design several smart materials, which exert the desired function in response to the specific biological environment, and then

ABSTRACT Multifunctional delivery systems of small interfering RNA (siRNA) are needed to overcome the intrinsic biological barriers toward efficient gene silencing in the cell cytoplasm. In this report, a smart

multilayered assembly (SMA) was fabricated by a layer-by-layer method with polyionic materials. The SMA was designed to feature a siRNA-loaded core, a transiently core-stabilizing silica interlayer, an endosome-disrupting polycation interlayer, and a biocompatible poly(ethylene glycol) (PEG) shell with reductive environment-responsive detachability. The SMA was confirmed to be approximately 160 nm in size with narrow distribution and spherical morphology by DLS and TEM analyses. The PEG detachability of the SMA based on disulfide cleavage was also confirmed by the increase in both ζ -potential and size due to the exposure of the polycation interlayer and the compromised colloidal stability. The silica interlayer rendered the SMA highly tolerant to dissociation induced by anionic lipids, while after 24 h dialysis siRNA release from the SMA was clearly observed, presumably due to gradual dissolution of the silica interlayer based on the equilibrium shift to silicate ions. The entrapment ratio of siRNA delivered by the SMA within the endosome was significantly lower than that by nondisulfide control (NDC) without PEG detachability, suggesting the improved endosomal escape of SMA with the exposed, endosome-disrupting interlayer after PEG detachment. SMAs induced significantly higher gene silencing efficiency in various cultured cells, compared to NDC, without associated cytotoxicity. The systemic administration of SMAs for subcutaneous tumor-bearing mice achieved significant endogenous gene silencing in tumor tissue without hematological toxicity.

KEYWORDS: siRNA delivery · polyion complex · silica · poly(ethylene glycol) · layer-by-layer



to integrate those component materials into one formulation toward multifunctionalities. For this purpose, construction of multilayered polyion complexes (PICs) by a layer-by-layer (LbL) technique allows the facile integration of a variety of charged components with different functionality as well as negatively charged nucleic acids into one nanoparticle.^{22–24} A few recent

* Address correspondence to kataoka@bmw.t.u-tokyo.ac.jp, miyata@bmw.t.u-tokyo.ac.jp.

Received for review March 16, 2012 and accepted July 26, 2012.

Published online July 26, 2012
10.1021/nm301164a

© 2012 American Chemical Society

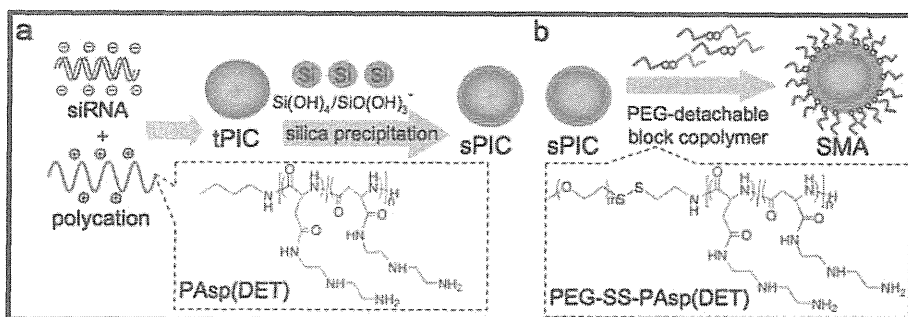


Figure 1. Preparation schemes of a smart multilayered assembly (SMA) by the layer-by-layer method. (a) Preparation of silica-coated PIC (sPIC) by silica-coating of the template PIC (tPIC). (b) Preparation of the SMA (PEG-SS-PAsp(DET)/silica-coated PAsp(DET)/siRNA PIC) by additional coating with PEG-block-polycation.

studies reported that the LBL technique successfully prepared siRNA-incorporating nano/microparticles from gold nanoparticle templates or mesoporous silica microparticle templates with several charged components for enhanced siRNA delivery.^{25–27}

For transient stabilization of PIC structures, the covering of their surface with a silica layer is one of the promising approaches, because the silica layer (i) can be easily prepared on the surface of cationic PICs, (ii) is negatively charged, thus available as a substrate for additional adsorption of the oppositely charged components, and (iii) substantially stabilizes the PIC, while gradually dissolving for payload release under highly dilute conditions based on the equilibrium shift to silicate ions.^{28,29} Indeed, our previous study revealed that the plasmid DNA-carrying PIC was successfully coated with a silica layer by simple incubation with sodium silicate solutions and was reversibly stabilized in a silicate concentration-dependent manner, leading to enhanced gene expression in cultured cells.²⁹ Meanwhile, for the preparation of biocompatible nanoparticles, installation of poly(ethylene glycol) (PEG) on their surface, termed PEGylation, is one of the most promising strategies. PEGylated nanoparticles are sterically stabilized by highly flexible and hydrated PEG chains, preventing the nanoparticles from secondary aggregate formation and nonspecific interactions with biomacromolecules, such as serum components and blood cells.^{30–32} However, in the case of nucleic acid delivery, such PEG shielding has concurrently compromised the membrane-disrupting (or endosomal escape) functionality of nanoparticles, resulting in lower transfection efficiency (termed PEG dilemma).³³ To bypass this dilemma, several previous studies, including ours, demonstrated the utility of PEG-detachable systems, which are constructed by smart block copolymers of PEG and an endosome-disrupting polycation tethered by cleavable linkers in the endosome/lysosome, *e.g.*, a reductive environment-responsive disulfide bond^{33,34} and an acidic pH-responsive hydrazone.³⁵ The PEG detachment within the endosome can expose the endosome-disrupting polycation on the nanoparticle surface for facilitated endosomal escape.

In the present study, a smart multilayered assembly (SMA) was developed with the PIC featuring a siRNA-loaded core, a transiently core-stabilizing silica interlayer, an endosome-disrupting polycation interlayer, and a detachable PEG shell, altogether aimed toward biocompatible and multifunctional siRNA delivery (Figure 1). The distinctive feature of this formulation was that SMAs were constructed with soft materials, *i.e.*, hydrophilic polymers and nonannealed silica. They can be metabolized more rapidly in the body compared to previous formulations prepared from iron, gold, or annealed mesoporous silica nanoparticles, thereby providing a great advantage for multiple-dose administration. As the endosome-disrupting polycation, a poly-aspartamide derivative bearing two repeating units of aminoethylene (termed PAsp(DET)) was selected and further tethered with PEG through a disulfide bond (–SS–), which can be cleaved by reducing enzymes on the cellular membrane or in the endosome/lysosome.^{36,37} PAsp(DET) has been extensively shown to induce strong membrane disruption selectively at endosomal acidic pH (~5.5) for efficient, less toxic endosomal escape, probably due to the distinctive change in the protonated structure in the side chain, *i.e.*, the monoprotonated state at extracellular pH 7.4 and the diprotonated state at acidic pH.^{38–42} The utility of SMAs was physicochemically and biologically investigated in comparison with the control without PEG detachability. In particular, the feasibility of SMAs for siRNA-based cancer therapy was examined with regard to endogenous gene silencing efficiency in a subcutaneous tumor model and also hematological toxicity after systemic administration. Ultimately, we demonstrate that SMAs may be promising formulations for successful siRNA delivery.

RESULTS AND DISCUSSION

Preparation and Physicochemical Characterization of the SMA. A SMA, that is, PEG-SS-PAsp(DET)/silica-coated PAsp(DET)/siRNA PIC, was prepared as illustrated in Figure 1. At first, the PAsp(DET)/siRNA-based template PIC (tPIC) was prepared by mixing siRNA with PAsp(DET) in a buffer solution (Figure 1a). A residual molar ratio of amines in PAsp(DET) to phosphate in siRNA = 3,

corresponding to a residual molar ratio of protonated amines in PAsp(DET) to phosphates in siRNA of 1.5,¹² was selected to obtain the positively charged tPIC with a minimal amount of unbound polycations for effective silica-coating. The formation of tPICs with a hydrodynamic size of 115 nm, a polydispersity index (PDI) of less than 0.1, and a positive ζ -potential (~ 20 mV) was confirmed with the Zetasizer (Table 1 and Figure 2a). It should be noted that PAsp(DET) was selected as a component polycation because of its considerably low cytotoxicity and excellent endosome-disrupting capability.^{38–42} In detail, the protonation state of the side chain of PAsp(DET) changes from a monoprotonated state to a diprotonated state in response to the endosomal acidification. The membrane-disrupting activity of PAsp(DET) is quite low in the monoprotonated state, but is significantly augmented in the diprotonated state for effective endosome disruption. Despite the excellent endosome-disrupting capability of PAsp(DET), the low stability of PAsp(DET)/siRNA PICs in serum-containing media has substantially limited their gene silencing efficiency,^{12,43,44} thereby requiring additional stabilization strategies for successful siRNA delivery.

According to the previously reported protocol,²⁹ silica-coating was performed by incubation of tPIC with sodium silicates in 10 mM HEPES buffer (pH 7.3) for 24 h at room temperature, then characterized with the Zetasizer. In the range of sodium silicate

concentrations above 3 mM, the obtained PICs showed almost the same sizes (~ 130 nm) and negative ζ -potentials (~ -20 mV) (Supporting Figure 2). Through incubation with silicates, the PIC size was considerably increased, and the ζ -potential was converted from the positive to the negative, well consistent with the formation of the anionic silica layer on the PIC surface. It should be noted that no leakage of siRNA from PICs was observed after silica-coating (Supporting Figure 3). The silica-coated PIC (sPIC) prepared at 3.5 mM sodium silicate was selected for the following experiments, as it exhibited the smallest size with relatively less silicates; at 3.5 mM sodium silicate sPICs had a hydrodynamic size of 125 nm, and a relatively narrow size distribution (PDI = 0.08) for a polymer-based self-assembly, a negative ζ -potential (-19 mV), and spherical morphology, as shown in dynamic light scattering (DLS) results (Table 1 and Figure 2a and b) and transmission electron microscopy (TEM) images (Figure 2d and Supporting Figure 5a).

Next, a smart polymer, PEG-SS-PAsp(DET), was utilized for the additional covering of sPIC for construction of the SMA (Figure 1b). Prior to addition of the polymer, the sPIC solution was applied to ultrafiltration (3000g, molecular weight cutoff: 300 000 Da) to remove the unbound silica species. Then, the purified sPIC solution was mixed with the polymer solution with varying concentrations, followed by 1 h incubation at room temperature. In the mixed solution, large aggregates (several μm in diameter) were formed in lower polymer concentrations ($<250 \mu\text{M}$ in polymer amine) (Supporting Figure 4), probably due to the diminished electrostatic repulsion between the sPICs through charge neutralization of the surface silica by polymer binding. With further increase in polymer concentration, the PIC size was gradually decreased, presumably because of effective PEG-shielding, and consequently the size change leveled off at around a residual amino group concentration of $400 \mu\text{M}$ (equivalent to 5 times the siRNA phosphates in the solution). Considering the

TABLE 1. Size and Polydispersity Index (PDI) of PICs in 10 mM HEPES Buffer (pH 7.3), Determined by Dynamic Light Scattering

| | diameter (nm) | PDI |
|------|---------------|-----------------|
| tPIC | 115 \pm 8 | 0.08 \pm 0.01 |
| sPIC | 125 \pm 13 | 0.08 \pm 0.01 |
| SMA | 159 \pm 8 | 0.10 \pm 0.03 |
| NDC | 159 \pm 10 | 0.08 \pm 0.03 |
| NPC | 143 \pm 15 | 0.14 \pm 0.04 |

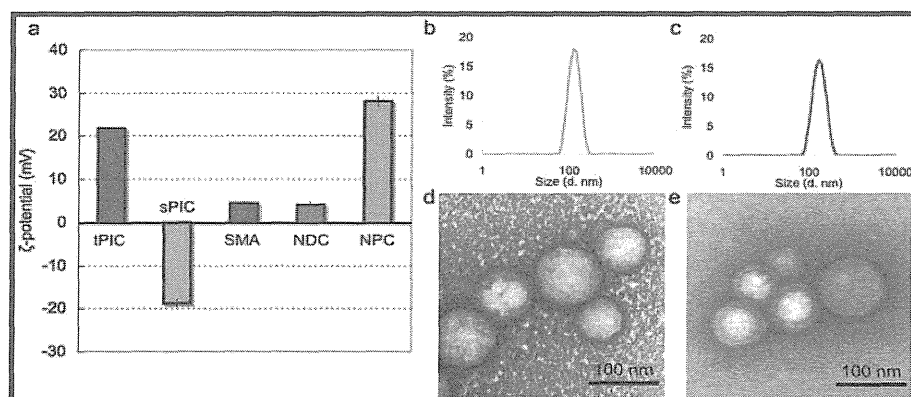


Figure 2. Physicochemical characterization of nanoparticle formulations. (a) ζ -Potential of PICs in 10 mM HEPES buffer (pH 7.3). (b, c) Intensity-based histograms of PICs determined by DLS: (b) sPIC and (c) SMA. (d, e) TEM images of PICs: (d) sPIC and (e) SMA (scale bar: 100 nm). PIC samples ($2 \mu\text{M}$ siRNA) were applied onto a copper TEM grid with carbon-coated collodion film and stained with uranyl acetate solution (2% w/v).

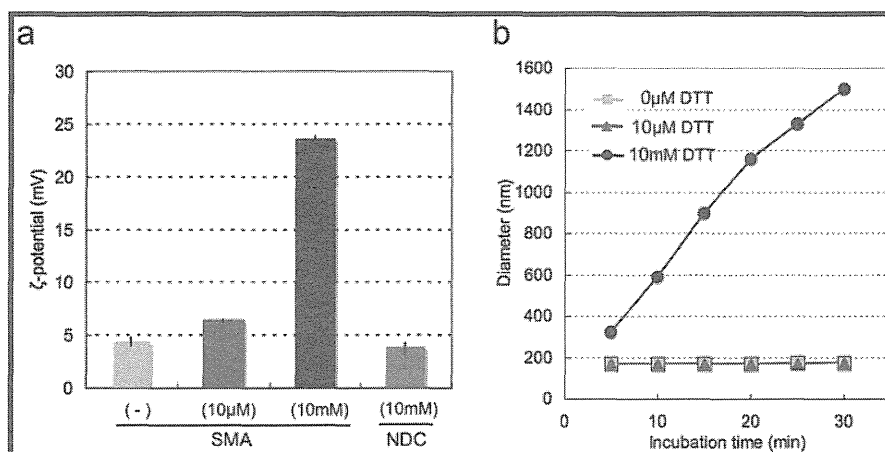


Figure 3. Reductive environment responsiveness of the SMA. (a) ζ -Potentials of the SMA and NDC after 30 min incubation in 10 mM HEPES buffer (pH 7.3) with or without DTT (0, 10 μ M and 10 mM DTT). Results are expressed as mean and standard deviation ($n = 3$). (b) Time-dependent change in size of the SMA in 10 mM HEPES buffer containing 150 mM NaCl (solid squares); in 10 mM HEPES buffer containing 150 mM NaCl and 10 μ M DTT (solid triangles); and in 10 mM HEPES buffer containing 150 mM NaCl and 10 mM DTT (solid circles), measured by DLS.

fact that an excess increase in polymer concentration may generate free (or uncomplexed) polymer in the solution, the sample prepared at a residual amino group concentration of 400 μ M was selected for further studies.

The hydrodynamic size and ζ -potential of a series of siRNA PICs are summarized in Table 1 and Figure 2a. A non-PEGylated control (NPC), which was prepared by mixing sPIC with PAsp(DET) homopolymer, had a hydrodynamic size of 143 nm with a PDI of 0.14 and a strongly positive ζ -potential of 28 mV, suggesting the formation of a cationic PAsp(DET) outer layer. In contrast, the SMA as well as the nondisulfide control (NDC), which was prepared from PEG-PAsp(DET), had a hydrodynamic size of 159 nm with the PDI of \sim 0.10 and a ζ -potential close to neutral (\sim 4 mV). The larger size ($P < 0.05$ for NPC) and the almost neutral ζ -potential of the SMA and NDC, compared with NPC, suggest that the sPIC should be successfully covered with a neutral PEG outer layer *via* the electrostatic interaction between anionic silica and the cationic PAsp(DET) segment of the block copolymers. Furthermore, the DLS and TEM histograms (Figure 2c and Supporting Figure 5b, respectively) and TEM images (Figure 2e and Supporting Figure 6) of the SMAs revealed that the relatively narrow size distribution and spherical morphology of sPICs were maintained. Note that the size distribution histograms obtained from TEM images were comparable to those from the number statistics of DLS (Supporting Figure 5).

Reductive Environment Responsiveness of the SMA. In order to examine the reductive environment-responsive PEG detachment from the SMA, the ζ -potential of the SMA was examined in 10 mM HEPES buffer (pH 7.3) containing different amounts of a reducing agent, dithiothreitol (DTT) (0, 10 μ M and 10 mM). Note that 10 μ M and 10 mM DTT were chosen to mimic the extracellular and the intracellular reducing potentials,

respectively, generated by glutathione.³⁶ In 10 mM HEPES buffer (pH 7.3), the SMA was observed to have a ζ -potential close to neutral (\sim 4 mV), suggesting the presence of a PEG shell that covers the nanoparticle. In contrast, after 30 min incubation in 10 mM HEPES buffer (pH 7.3) containing 10 mM DTT, the SMA exhibited an appreciably increased ζ -potential (24 mV), comparable to NPC, whereas a much lower ζ -potential was observed in the 10 μ M DTT condition (Figure 3a). The appreciably increased ζ -potential of the SMA in the stronger reductive condition is well consistent with the exposure of the positively charged PAsp(DET) layer due to the PEG detachment based on the disulfide cleavage. The pivotal role of the disulfide bond for PEG detachment in the SMA is also suggested by the result that the NDC maintained the neutral ζ -potential even in the stronger reductive conditions (Figure 3a). The PEG detachability in the SMA was further examined from the standpoint of the colloidal stability of the nanoparticles. DLS measurement was conducted to monitor the size change of SMAs as well as NDCs and NPCs in 10 mM HEPES buffer (pH 7.3) containing 150 mM NaCl. First, the NDC and NPC were compared to estimate the effect of PEG on the size change. The size of the NPCs clearly increased over the incubation period, reaching μ m dimensions in 30 min, presumably due to secondary aggregate formation under the physiological salt conditions, which attenuates the electrostatic repulsion between the charged nanoparticles (Supporting Figure 7). In contrast, this secondary aggregate formation was dramatically suppressed in the NDC formulation (Supporting Figure 7), demonstrating the enhanced colloidal stability of PICs with PEG palisades. Next, the SMAs were similarly evaluated by DLS in the same buffer with or without DTT (Figure 3b). At 0 and 10 μ M DTT, no size change of the SMAs was observed following 30 min incubation, similar to NDCs, indicating that the colloidal stability of

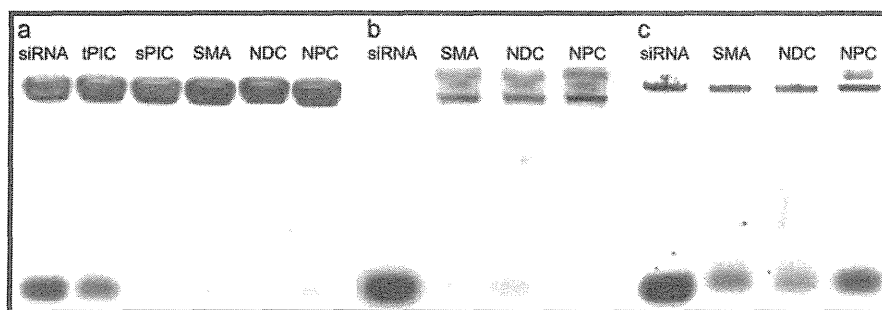


Figure 4. Tolerability of PICs against dissociation triggered by anionic lipids. siRNA release from PICs was evaluated by agarose gel electrophoresis. (a) Each PIC was incubated in 10 mM HEPES buffer (pH 7.3) containing anionic lipids, DOPS, for 48 h at a molar ratio of carboxyl groups in DOPS to phosphate groups in siRNA of 32. (b, c) Each PIC solution was dialyzed (molecular weight cutoff: 5000 Da) against a 1000-fold excess of 10 mM HEPES buffer (pH 7.3) for (b) 3 h and (c) 24 h. Then, each PIC solution was mixed with DOPS and incubated for 24 h, followed by electrophoresis.

the SMA was maintained even in mild reductive conditions. In sharp contrast, in the conditions containing 10 mM DTT, the increase in size of the SMA was clearly observed over the incubation period, similar to NPC (Supporting Figure 7), indicating the significantly compromised colloidal stability presumably due to the PEG detachment. Altogether, the PEG palisade in the SMA may sterically stabilize siRNA PICs in extracellular conditions, but can be removed on the cellular surface and/or in the endosome/lysosome with higher reducing potentials,^{36,37} to expose the endosome-disrupting PAsp(DET) layer.

Stability Shift in the SMA with a Dissolvable Silica Interlayer.

When administered in the body, siRNA PICs encounter abundant charged biomolecules, such as serum proteins and cell membranes, which may nonspecifically bind to the PICs, possibly leading to undesirable dissociation. Thus, high resistance toward such dissociation is a prerequisite for *in vivo* applications of siRNA PICs. In addition, once delivered into the cytoplasm, siRNA must also be released from PICs to allow association with RNAi-related proteins. Integration of a silica layer onto siRNA PICs should be a promising solution to overcome this conflicting requirement, because the silica layer stabilizes the siRNA PICs while also dissolving in a time-dependent manner in dilute conditions based on the equilibrium shift in the silicate ions.^{29,45}

To investigate the stability shift induced by silica dissolution, the SMA was challenged by an anionic lipid, 1,2-dioleoyl-*sn*-glycero-3-phospho-L-serine sodium salt (DOPS),⁴⁶ before and after dialysis against a 1000-fold volume of 10 mM HEPES buffer (pH 7.3) for 3 and 24 h for removal of generated free silicates. Note that DOPS was selected as a model anionic molecule in this assay, as phosphatidylserine is one of the major components of cell membranes that can interact with siRNA PICs in intracellular conditions, thereby is useful for estimation of the feasibility of siRNA release from PICs in cells. Each sample was incubated with DOPS (the mixing ratio was set at a molar ratio of carboxyl groups in DOPS to phosphate groups in siRNA of 32), followed by agarose gel electrophoresis. As shown in

Figure 4a, the band corresponding to naked siRNA was clearly observed for the tPIC sample incubated with DOPS, indicating PIC dissociation. In contrast, siRNA release was significantly suppressed for the SMA formulation as well as sPICs before dialysis. Thus, it was confirmed that the silica layer rendered siRNA PICs highly tolerant to counteranion-triggered dissociation. On the other hand, siRNA was considerably released from SMAs after dialysis for 24 h (Figure 4c), whereas release was still limited after dialysis for 3 h (Figure 4b). Note that a similar tendency was also observed for NDCs and NPCs featuring a silica layer (Figure 4a–c). These results demonstrate that the dissolvable silica layer in siRNA PICs can induce a stability shift for smooth release of siRNA in the cytoplasm.

Gene Silencing and Cell Viability Assays. The efficiency of gene silencing was evaluated using a luciferase assay against HuH7-Luc, a human hepatoma cell stably expressing luciferase. A linear polyethyleneimine-based transfection reagent (ExGen 500) was used as a positive control in this assay. As shown in Figure 5a, the SMA as well as NDC and NPC appreciably enhanced the gene silencing efficiency at higher siRNA concentrations, compared to tPIC and sPIC, suggesting that PAsp(DET)-based polymers bound onto a sPIC surface improved the siRNA delivery efficiency. Although there was no significant difference between SMAs and NDCs at the lowest siRNA concentration tested, the SMAs exerted significantly higher gene silencing efficiency than NDCs at higher siRNA concentrations ($P < 0.01$ at 200, 300, and 400 nM siRNA), suggesting that the enhanced efficiency of the SMA should be due to the PEG detachability. The exposure of the PAsp(DET) layer after the PEG detachment may improve the endosomal escape efficiency of siRNA PICs. On the other hand, the gene silencing efficiency of the SMAs was lower than that of NPCs as well as ExGen 500 (Figure 5a), probably due to more efficient cellular uptake of the non-PEGylated PICs, as shown in the next section. Despite lower gene silencing efficiency, the SMA formulation with PEG palisades is more suitable for systemic administration *in vivo*, because the much lower colloidal

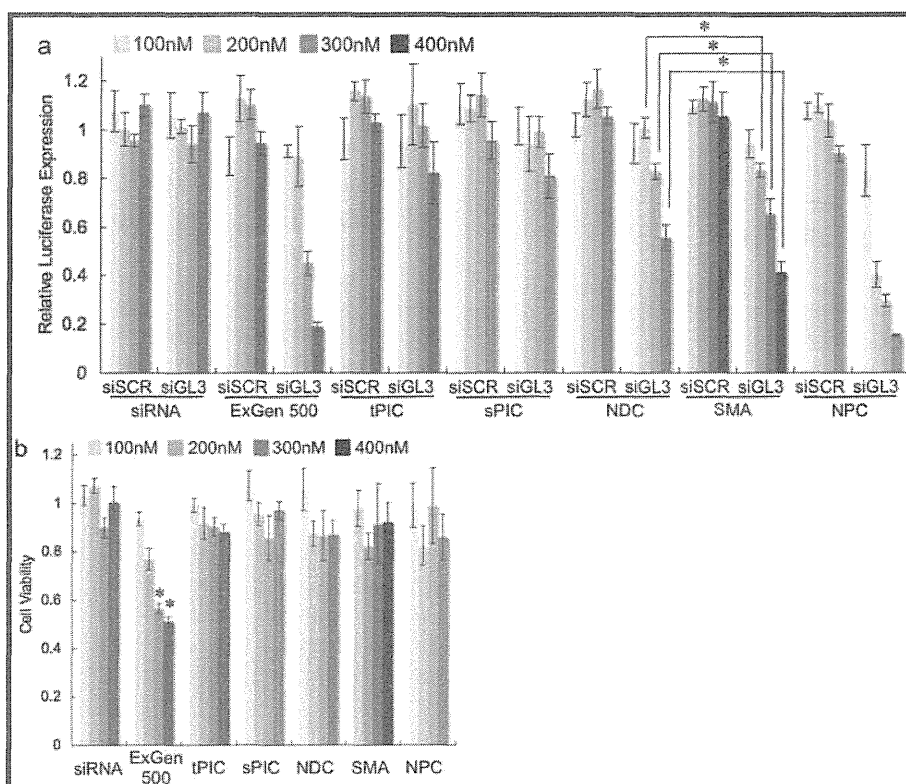


Figure 5. (a) Gene silencing activity against HuH7-Luc cells. Scramble siRNA (siSCR) was used as a control sequence for GL3 luciferase siRNA (siGL3). HuH7-Luc cells were treated with each PIC for 48 h (siRNA concentrations from the left: 100, 200, 300, and 400 nM) and subjected to the luciferase assay. Relative luciferase expression was calculated as the ratio of luciferase expression relative to nontreated cells. Results are expressed as mean and standard deviation ($n = 4$). $*P < 0.01$ for NDC. (b) Cell viability of HuH7-Luc cells in the same conditions as the gene silencing study was determined with the Cell Counting Kit-8 assay, with the cell viability of the nontreated cells set to 1. Results are expressed as mean and standard deviation ($n = 8$). $*P < 0.01$ compared to other samples. In both experiments, ExGen 500 was used according to the manufacturer's protocol as a commercially available positive control.

stability and strong positive ζ -potential of the non-PEGylated PICs would likely lead to the formation of secondary aggregates through nonspecific interactions with biomacromolecules during blood circulation.³² Note that a similar profile in gene silencing efficiency was also observed in other luciferase-expressing cell lines, human lung cancer (A549-Luc) and human ovarian cancer (SKOV3-Luc) (Supporting Figure 8). Meanwhile, all the PAsp(DET)-based PICs (tPIC, sPIC, NDC, SMA, and NDC) did not show substantial toxicity in cultured cells, which was in sharp contrast to ExGen 500 (Figure 5b). Reduced cytotoxicity of PAsp(DET)-based formulations is consistent with the previous reports of nucleic acid delivery using PAsp(DET), which features a monoprotinated state in each side chain at an extracellular neutral pH with appreciably less cytoplasmic membrane damage compared to other polycations, such as polyethyleneimine.^{12,40–42} Thus, the SMA is demonstrated to enhance the siRNA delivery efficiency without increasing the cytotoxicity.

Cellular Uptake and Intracellular Distribution Studies. The mechanism of the enhanced gene silencing achieved by the SMA was further investigated in comparison with the controls (NDC and NPC as well as sPIC).

To quantify the cellular uptake of each siRNA PIC by HuH7-Luc cells, the cells were incubated with the PICs prepared from Cy3-labeled siRNA (Cy3-siRNA) for 24 h and then subjected to flow cytometric analysis. As shown in Figure 6, the cellular uptake of Cy3-siRNA PICs was increased in the polymer/silica-coated systems (SMA, NDC, and NPC), compared to sPIC. In detail, the Cy3-siRNA uptake of the SMA was significantly higher than that of sPIC ($P < 0.05$) and significantly less than that of NPC ($P < 0.01$), whereas no statistical difference was observed between PEGylated systems (SMA and NDC) ($P > 0.05$). The observed cellular uptake profile was apparently correlated with the surface charge of PICs; higher fluorescence (or cellular uptake) was obtained by the PICs showing a higher ζ -potential (Figure 2a), possibly due to the fact that the positively charged surface should facilitate an association with the anionic cytoplasmic membrane.^{47,48} It should be noted that NPCs are likely to form secondary aggregates in the cell culture medium due to their lower colloidal stability (Supporting Figure 7), possibly affecting the cellular association and uptake. The significantly limited uptake efficiency observed for the SMA, compared to NPC, suggests that the PEG shell in the SMA might be effectively maintained during

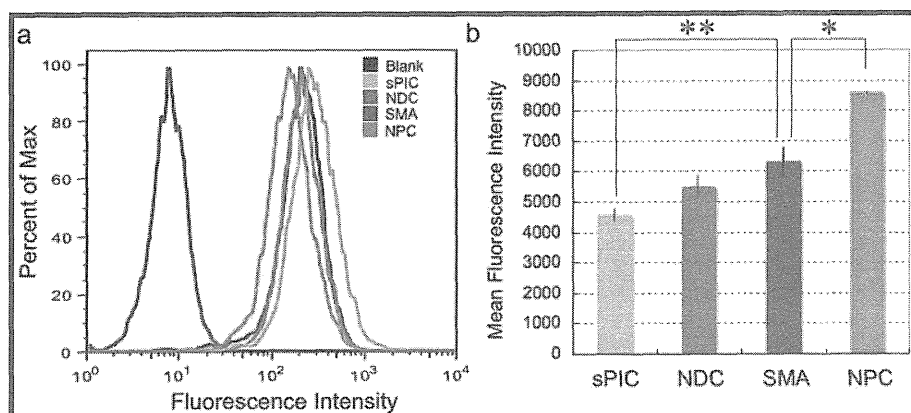


Figure 6. Cellular uptake of Cy3-siRNA PICs evaluated by flow cytometric analysis. HuH7-Luc cells were incubated with each PIC (siRNA concentration: 400 nM) for 24 h. (a) Flow cytometric data shown in the histogram. (b) Flow cytometric data shown in the bar graph. Results are expressed as mean and standard deviation ($n = 3$). * $P < 0.01$ for NPC. ** $P < 0.05$ for sPIC.

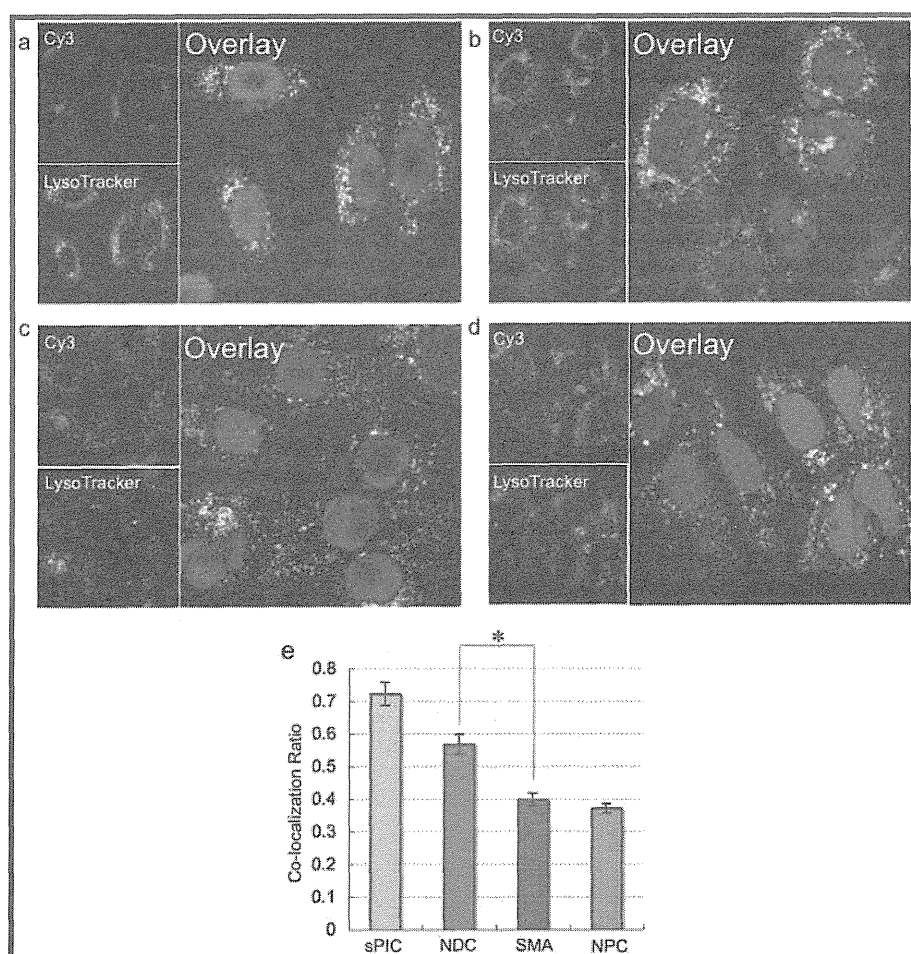


Figure 7. Intracellular distribution of Cy3-siRNA PICs. (a–d) CLSM images of (a) sPIC, (b) NDC, (c) SMA, and (d) NPC (red: Cy3-siRNA, green: LysoTracker Green, blue: Hoechst33342). HuH7-Luc cells were incubated with each PIC at 400 nM siRNA for 24 h. (e) Co-localization ratio of Cy3-siRNA with the late endosome/lysosome marker (LysoTracker Green) calculated from the number of pixels in the obtained CLSM images. Results are expressed as mean and standard deviation ($n = 20$). * $P < 0.01$ for NDC.

incubation in the cell culture medium. The facilitated cellular uptake in the polymer/silica-coated systems, especially in NPC, might contribute to their enhanced gene silencing efficiency (Figure 5a). Nevertheless, the similar uptake efficiency between the SMA and NDC also suggests that there is another crucial factor to

explain their significantly different gene silencing efficiency (Figure 5a), as demonstrated by the following confocal laser scanning microscopic (CLSM) analysis.

Once endocytosed by cells, siRNA PICs were generally transported to the late endosome/lysosome, which is the digestive organelle. Thus, the efficient

endosomal escape of PICs is critical for successful siRNA delivery into the cytoplasm. Herein, the intracellular distribution of Cy3-siRNA PICs was observed using CLSM after 24 h incubation with the cells. In the obtained CLSM images, the signals from Cy3-siRNA, LysoTracker Green, and Hoechst33342 are shown in red, green, and blue, respectively (Figure 7a–d). The endosomal entrapment efficiency was further estimated by calculating the number ratio of the pixels of Cy3-siRNA co-localizing with the late endosome/lysosome marker (yellow) to all the pixels of Cy3-siRNA (yellow and red). Obviously, the co-localization ratios in the polymer/silica-coated systems (SMA, NDC, and NPC) were lower than that in sPIC (Figure 7e), indicating that efficient endosomal escape should be induced by the coating of sPIC with PAsp(DET)-based polymers. Notably, the SMA featuring the detachable PEG shell showed a significantly lower co-localization ratio than NDC ($P < 0.01$), suggesting that reductive environment-responsive PEG detachment (Figure 3) might accelerate the endosomal escape of the SMA for the significantly enhanced gene silencing efficiency (Figure 5a).

Therapeutic Gene Silencing *in Vitro* and *in Vivo*. To further examine the potential utility of the SMA formulation for siRNA-based cancer therapy, the gene silencing ability

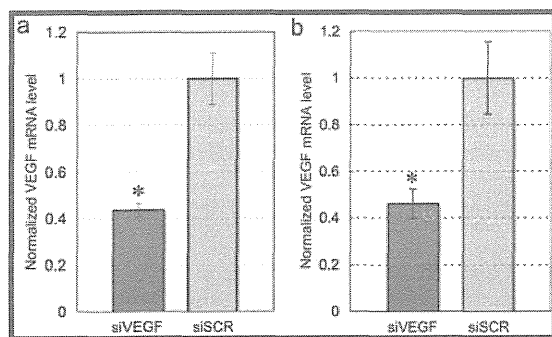


Figure 8. (a) *In vitro* VEGF gene silencing activity of SMAs in OS-RC-2 cells determined by RT-PCR. OS-RC-2 cells were incubated with SMAs for 48 h (siRNA concentration: 200 nM) prior to RT-PCR analysis. (b) *In vivo* VEGF gene silencing activity of SMAs in subcutaneous OS-RC-2 tumors. SMAs were intravenously injected into mice (1.25 mg siRNA/kg mouse) at days 1 and 2, and at day 3 subcutaneous tumors were excised and total RNA was extracted. In both *in vitro* and *in vivo* experiments, the level of VEGF mRNA was normalized to actin mRNA, and scramble siRNA (siSCR) was used as a control sequence for VEGF siRNA (siVEGF). Results are expressed as mean and standard error of the mean ($n = 4$). * $P < 0.05$ compared to siSCR.

of SMAs was investigated *in vitro* and *in vivo* for a therapeutic gene targeting the human renal cancer cell line OS-RC-2. Treatment of renal cancer with siRNA is a particularly attractive therapeutic target, as highly effective clinical anticancer drugs are currently unavailable. Vascular endothelial growth factor (VEGF) was selected as the target gene, because VEGF is a proangiogenic molecule that is overexpressed in a wide variety of cancer cells to stimulate angiogenesis and tumor growth.⁴⁹ To date, several previous studies demonstrated that VEGF gene silencing in tumor tissues significantly inhibits tumor growth.^{34,50–53} Thus, the gene silencing ability of SMAs containing siRNA targeted toward VEGF (siVEGF) was examined in cultured OS-RC-2 cells by real-time reverse transcriptional PCR (RT-PCR). As shown in Figure 8a, SMAs containing siVEGF significantly reduced the VEGF mRNA level (~57%), compared to control SMAs containing scramble siRNA (siSCR).

Next, the *in vivo* gene silencing activity of siRNA delivered in SMAs was investigated using a subcutaneous OS-RC-2 tumor model following systemic administration by tail vein injection (1.25 mg siRNA/kg mouse). Prior to the gene silencing assay, several hematological parameters of mice treated with SMAs containing siSCR were monitored 24 h after systemic administration as indices of *in vivo* toxicity. Analysis of hematological parameters revealed that systemically administered SMA induced no problematic hematological toxicity (Table 2). For *in vivo* gene silencing assays, each mouse was injected twice at days 1 and 2, and at day 3 subcutaneous tumors were excised and RNA was extracted for RT-PCR. Figure 8b clearly shows that systemic administration of SMAs containing siVEGF induced significant reduction in the VEGF mRNA level (~50%) in the tumor tissue, compared to the control containing siSCR ($P < 0.05$), demonstrating the sequence-specific gene silencing ability of siRNA delivered by SMAs. Altogether, these results demonstrate the strong potential of SMAs for systemic siRNA delivery to tumor tissues without adverse side effects.

CONCLUSIONS

In this study, a smart multilayered assembly was prepared by a layer-by-layer method with PICs to feature a siRNA-loaded core, a transiently core-stabilizing silica interlayer, an endosome-disrupting PAsp(DET) interlayer, and a detachable PEG shell for

TABLE 2. Hematological Parameters of Mice Treated with SMA^a

| | siRNA dose (mg/kg) | ALT (U/L) | AST (U/L) | RBC ($\times 10^5/\mu\text{L}$) | WBC ($\times 10^2/\mu\text{L}$) | hemoglobin (g/dL) |
|----------------|--------------------|------------|------------|-----------------------------------|-----------------------------------|-------------------|
| buffer control | 0 | 48 \pm 4 | 54 \pm 2 | 100 \pm 2 | 27 \pm 4 | 14.4 \pm 0.3 |
| SMA | 1.25 | 43 \pm 5 | 49 \pm 4 | 97 \pm 4 | 30 \pm 4 | 14.4 \pm 0.5 |

^a Blood samples ($n = 4$) were collected 24 h after systemic administration. ALT, alanine aminotransferase; AST, aspartate aminotransferase; RBC, red blood cells; WBC, white blood cells.

multifunctional siRNA delivery. The successful preparation was confirmed by the change in size and ζ -potential of the PICs as well as their TEM images. The PEG detachability of the SMA in response to the reductive conditions was also confirmed by the change in size (or colloidal stability) and ζ -potential. The silica interlayer in the SMA substantially improved the tolerability of siRNA PICs to the dissociation triggered by the anionic lipids, while significant siRNA release was induced after the dialysis for removal of generated free silicates, indicating the dissolvable nature of the silica interlayer. SMAs significantly enhanced gene silencing for not only a reporter gene but also an

endogenous therapeutic gene (VEGF) in cultured cancer cells without increased cytotoxicity. The major mechanism for the enhanced gene silencing in SMA was probably the facilitated endosomal escape of siRNA PICs through endosome disruption by the exposed PAsp(DET) layer after PEG detachment. Ultimately, systemic administration of SMAs into subcutaneous tumor-bearing mice resulted in significant VEGF gene silencing in the tumor tissue without problematic hematological toxicity. These results demonstrate the potential utility of the SMA formulation for systemic siRNA delivery aimed toward cancer therapy.

MATERIALS AND METHODS

Materials. α -Methoxy- ω -mercapto poly(ethylene glycol) (PEG-SH, $M_n = 10\,000$) and α -methoxy- ω -amino poly(ethylene glycol) (PEG-NH₂, $M_n = 12\,000$) were obtained from NOF Co. (Tokyo, Japan). β -Benzyl L-aspartate N-carboxy anhydride (BLA-NCA) was purchased from Chuo Kaseihin Co., Inc. (Tokyo, Japan). Methanol (MeOH), 2-aminoethanethiol, benzene, hexane, ethyl acetate, *N,N*-dimethylformamide (DMF), dichloromethane (DCM), diethylenetriamine (DET), *N*-methyl-2-pyrrolidone (NMP), *n*-butylamine, and dithiothreitol (DTT) were purchased from Wako Pure Chemical Industries, Ltd. (Osaka, Japan). DMF, DCM, NMP, *n*-butylamine, and DET were distilled before use. Dulbecco's modified Eagle's medium (DMEM) was purchased from Sigma Aldrich (St. Louis, MO, USA). Fetal bovine serum (FBS) was purchased from Dainippon Sumitomo Pharma Co, Ltd. (Osaka, Japan). Sterile HEPES (1 M, pH 7.3) was purchased from Amresco (Solon, OH, USA). The luciferase assay system was purchased from Promega Co. (Madison, WI, USA). All the RNA molecules, including 5'-Cy3-labeled RNA, were synthesized by Hokkaido System Science (Hokkaido, Japan). The sequences are as follows: GL3 luciferase siRNA (sense: 5'-(Cy3)-CUU ACG CUG AGU ACU UCG AdTdT-3', antisense: 5'-UCG AAG UAC UCA GCG UAA GdTdT-3'), human VEGF siRNA (sense: 5'-GAU CUC AUC AGG GUA CUC CdTdT-3', antisense: 5'-GGA GUA CCC UGA UGA GAU CdTdT-3'), and scramble siRNA (sense: 5'-UUC UCC GAA CGU GUC ACG UdTdT-3', antisense: 5'-ACG UGA CAC GUU CGG AGA AdTdT-3').

Synthesis of PEG-SS-NH₂. α -Methoxy- ω -dithioamino poly(ethylene glycol) (PEG-SS-NH₂) was synthesized as previously described.³³ In brief, PEG-SH (3.75 g, 0.375 mmol) was dissolved in methanol (400 mL) containing 28% sodium methoxide. 2-Aminoethanethiol (4.23 g, 37.3 mmol) was added to the PEG-SH solution, and the mixture was stirred for 5 days at room temperature. Then, the reaction solution was neutralized with cold 5 N HCl (8.15 mL, 40.8 mmol), followed by dialysis against distilled water for 1 day. The dialyzed solution was further purified through the ion-exchange resin (SP-Sephadex C-50, solute: H₂O), followed by lyophilization to obtain PEG-SS-NH₂ as a chloride salt form. Finally, PEG-SS-NH₂Cl dissolved in deionized water was dialyzed against 0.1% NH₃ solution for 1 day to deprotonate the amino group of the PEG-SS-NH₂. Then, the sample (PEG-SS-NH₂) was lyophilized and collected (2.76 g, 0.276 mmol).

Synthesis of PEG-SS-PBLA, PEG-PBLA, and PBLA. Poly(ethylene glycol)-disulfide-poly(β -benzyl L-aspartate) (PEG-SS-PBLA), poly(ethylene glycol)-poly(β -benzyl L-aspartate) (PEG-PBLA), and poly(β -benzyl L-aspartate) (PBLA) were synthesized by the ring-opening polymerization of BLA-NCA initiated by PEG-SS-NH₂, PEG-NH₂, and *n*-butylamine, respectively, according to the previously described method.³³ The typical synthetic procedure is briefly shown for PEG-SS-PBLA. PEG-SS-NH₂ (0.40 g, 0.04 mmol) and BLA-NCA (1.08 g, 4.32 mmol) were dissolved in DCM (6.0 mL) and DMF (1.5 mL), respectively. The solution

containing BLA-NCA was added to the PEG-SS-NH₂ solution and stirred at 35 °C under an argon atmosphere. After 48 h, the reaction solution was precipitated in hexane/ethyl acetate (6:4 v/v) and dried overnight under reduced pressure to obtain PEG-SS-PBLA (1.12 g, yield 87%). In order to determine the molecular weight distribution (M_w/M_n) of the obtained polymer, size exclusion chromatography (SEC) was performed using a TOSOH HLC-8820 equipped with TSK gel columns (SuperAW4000 and SuperAW3000 \times 2, TOSOH, Japan) and an internal refractive index detector at a flow rate of 0.3 mL min⁻¹ at 40 °C. NMP with 10 mM LiBr was used as an eluent. A narrow M_w/M_n (= 1.10) was confirmed from the SEC (data not shown). PEG-PBLA and PBLA were synthesized in a similar manner; e.g., BLA-NCA (840 mg, 3.36 mmol) and PEG-NH₂ (370 mg, 0.03 mmol) for PEG-PBLA (926 mg, yield 93%); and BLA-NCA (1.40 g, 4.86 mmol or 1.21 mg, 4.20 mmol) and *n*-butylamine (6.00 mL, 0.0607 mmol or 2.93 μ L, 0.0296 mmol) for PBLA with different degrees of polymerization (DPs) (888 mg, yield 77% or 910 mg, yield 91%), respectively. The DPs of the PBLA segment in PEG-SS-PBLA and PEG-PBLA were calculated to be 87 and 92, respectively, from the peak intensity ratio of the PEG protons to the benzyl protons (C₆H₅CH₂-, $\delta = 5.1$ and 7.3 ppm) at the side chain, and the DPs of two PBLAs were determined to be 92 and 225 from the peak intensity ratio of the butyl protons (CH₂CH₂CH₂CH₂-, $\delta = 0.8$ –1.5 ppm) at the α -chain end to the benzyl protons (C₆H₅CH₂-, $\delta = 5.1$ and 7.3 ppm) at the side chain in the ¹H NMR spectrum (polymer concentration: 10 mg/mL, solvent: dimethyl sulfoxide-*d*₆, temperature: 80 °C) (data not shown).

Synthesis of PEG-SS-PAsp(DET), PEG-PAsp(DET), and PAsp(DET). Introduction of a *N'*-[*N*-(2-aminoethyl)-2-aminoethyl] moiety into the polyaspartamide side chain was performed by the aminolysis reaction of benzyl groups of the PBLA segment with DET as previously described.³³ Briefly, a typical synthetic procedure is shown for poly(ethylene glycol)-disulfide-poly{*N'*-[*N*-(2-aminoethyl)-2-aminoethyl]aspartamide} (PEG-SS-PAsp(DET)). PEG-SS-PBLA (200 mg, 7 μ mol) lyophilized from a mixed solution of DCM (5 mL) and benzene (20 mL) was dissolved in NMP (10 mL) under an argon atmosphere. DET (3.44 mL, 32 mmol, 50 equiv to benzyl group in PEG-SS-PBLA) was dissolved in NMP (3.44 mL). The PEG-SS-PBLA solution was then added to the cooled DET solution and stirred at 4 °C for 1 h under an argon atmosphere. The reaction solution was added dropwise into cold 5 N HCl_{aq} (19.2 mL, 96 mmol) for neutralization and subsequently dialyzed against 0.01 M HCl_{aq} for 24 h and deionized water for an additional 24 h using a dialysis membrane (molecular weight cutoff: 6000–8000 Da). The dialyzed solution was lyophilized to obtain PEG-SS-PAsp(DET) as a hydrochloride salt (170 mg, yield 70%). Poly(ethylene glycol)-poly{*N'*-[*N*-(2-aminoethyl)-2-aminoethyl]aspartamide} (PEG-PAsp(DET)) and poly{*N'*-[*N*-(2-aminoethyl)-2-aminoethyl]aspartamide} (PAsp(DET)) were synthesized in a similar manner, e.g., PEG-PBLA (103 mg, 3.20 μ mol) and DET (1.5 mL, 14.7 mmol) for PEG-PAsp(DET) (98.0 mg, yield 85%); and PBLA (149 mg, 7.90 μ mol)

and DET (3.9 mL, 38.2 mmol) for PAsp(DET) (182 mg, yield 91%). The quantitative conversion of PBLA to PAsp(DET) in PEG-SS-PAsp(DET) and PEG-PAsp(DET) was confirmed from the peak intensity ratio of the protons of the PEG chain ($-(CH_2)_2-O-$, $\delta = 3.7$ ppm) to those of the ethylene unit in the 1,2-diaminoethane ($H_2N(CH_2)_2NH(CH_2)_2NH-$, $\delta = 3.1-3.5$ ppm) moieties in the side chain of PAsp(DET) in the 1H NMR spectra (polymer concentration: 10 mg/mL, solvent: D_2O , temperature: 80 °C) (Supporting Figure 1a and b, respectively). In the case of PAsp(DET), the quantitative conversion was confirmed from the peak intensity ratio of the protons of the butyl group at the α -chain end ($CH_3CH_2CH_2CH_2-$, $\delta = 0.8-1.5$ ppm) to the ethylene protons in the 1,2-diaminoethane ($H_2N(CH_2)_2NH(CH_2)_2NH-$, $\delta = 3.1-3.5$ ppm) moieties in the side chain of PAsp(DET) in the 1H NMR spectra (polymer concentration: 10 mg/mL, solvent: D_2O , temperature: 80 °C) (Supporting Figure 1c and d).

Preparation of a Series of PICs. PAsp(DET) (DP = 225) was dissolved in 10 mM HEPES buffer (pH 7.3) at a concentration of 5 mg/mL. Then, the PAsp(DET) solution was mixed with 15 μ M siRNA (10 mM HEPES buffer, pH 7.3) to obtain an siRNA-incorporating PIC (final siRNA concentration: 2 μ M). The residual molar ratio of amines in PAsp(DET) to phosphates in siRNA in the PIC solution was set to 3 to obtain a slightly positive PIC without an excess amount of polycations. After 30 min incubation at 4 °C, varying concentrations of sodium silicate solutions (10 mM HEPES buffer (pH 7.3)) were added to the PIC solution (final siRNA concentration: 1 μ M). After 24 h incubation at room temperature, the mixed solution was purified by ultrafiltration (3000g, molecular weight cutoff: 300,000 Da) to remove the unbound silica species. Then, the purified solutions were mixed with the solution containing PEG-SS-PAsp(DET), PEG-PAsp(DET), or PAsp(DET) (DP = 92) (final siRNA concentration: 2 μ M), followed by incubation at 25 °C for 1 h to obtain polymer/silica-coated PICs.

Size and ζ -Potential Measurements. The size and ζ -potential of each PIC were measured using a Zetasizer Nano-ZS instrument (Malvern Instruments, Malvern, UK) equipped with a He-Ne ion laser ($\lambda = 633$ nm) as an incident beam at a detection angle of 173° and at a temperature of 25 °C. In DLS, each PIC solution (20 μ L, 1 μ M siRNA, 10 mM HEPES buffer (pH 7.3) with or without 150 mM NaCl) was added into a low-volume cuvette (Malvern Instruments, Malvern, UK) for the measurements. The cumulant method was used to analyze the data obtained from the decay in the photon correlation function to obtain the hydrodynamic diameters and polydispersity indices. The results were shown as mean and standard deviation of the mean obtained from eight samples.

For ζ -potential measurement, each sample (700 μ L, 1 μ M siRNA, 10 mM HEPES buffer (pH 7.3)) was put into a folded capillary cell (Malvern Instruments, Malvern, UK). The obtained electrophoretic mobility was converted to the ζ -potential by applying the Smoluchowski equation: $\zeta = 4\pi\eta\nu/\epsilon$ (η : viscosity of the solvent, ν : electrophoretic mobility, ϵ : dielectric constant of the solvent). The results were shown as mean and standard deviation obtained from three samples.

Transmission Electron Microscopic Observation. TEM observation was conducted using an H-7000 electron microscope (Hitachi, Tokyo, Japan) operated at 75 kV acceleration voltage. Copper TEM grids with carbon-coated collodion film were glow-discharged for 10 s using an Eiko IB-3 ion coater (Eiko Engineering Co. Ltd., Japan). The grids were dipped into PIC solution (2 μ M siRNA), which was mixed with uranyl acetate solution (2% w/v) for 60 s. After removal of excess solution with a filter paper, the sample grids were allowed to dry in air and then TEM observation was performed.

Agarose Gel Electrophoresis. siRNA release from PICs caused by an anionic lipid, 1,2-dioleoyl-*sn*-glycero-3-phospho-L-serine sodium salt, was evaluated by agarose gel electrophoresis for estimation of the PIC stability. Each PIC solution (2 μ M siRNA) was mixed with DOPS solution (2 mg/mL) at a molar ratio of carboxyl groups in DOPS to phosphate groups in siRNA of 32. After 48 h incubation at room temperature, the mixed solutions were subjected to electrophoresis by 0.9 wt % agarose gel in the TAE buffer (pH 7.4). siRNA in the gel was stained by ethidium

bromide and analyzed by an FX molecular imager (BIO-RAD) equipped with Quantity One software (BIO-RAD).

Gene Silencing Assay. The gene silencing efficiency of the PICs was evaluated from the luciferase-based luminescence intensity of luciferase-expressing human hepatoma cells, HuH7-Luc. The cells were plated on a 48-well plate at a cell density of 5000 cells/well in DMEM supplemented with 10% FBS and incubated for 24 h. Then, the old medium was replaced with fresh medium, and PICs were added at a concentration of 100, 200, 300, and 400 nM siRNA. After 48 h incubation, the PIC-containing medium was removed. After washing with 100 μ L of PBS, the cells were lysed with 100 μ L of the cell culture lysis buffer (Promega). The luciferase expression in the lysate was measured using a luciferase assay system (Promega) and a luminescence microplate reader (Mithras LB 940, Berthold Technologies, Bad Wildbad, Germany). The relative luciferase expression of the cells treated with PICs was calculated as a ratio of the expression of nontreated cells. The results were expressed as mean and standard deviation obtained from four samples.

Cell Viability Assay. HuH7-Luc cells were plated on a 48-well plate at a cell density of 5000 cell/well in DMEM supplemented with 10% FBS. After incubation for 24 h, the old medium was replaced with fresh medium, and the PICs were applied at a concentration of 100, 200, 300, and 400 nM siRNA. After 48 h incubation, the cell viability assay was performed using Cell Counting Kit-8 with WST-8, a soluble tetrasolium salt, according to the manufacturer's protocol (Dojindo, Japan). The absorbance was measured using a microplate reader with a filter of 450 nm (model 680, BIO-RAD). The cell viability was determined as a percentage of the absorbance of nontreated cells. The results were expressed as mean and standard deviation obtained from eight samples.

Flow Cytometric Analysis. HuH7-Luc cells were plated on a 12-well plate at a cell density of 25 000 cells/well in DMEM supplemented with 10% FBS and incubated for 24 h. The PICs prepared from Cy3-siRNA were applied to each well at a concentration of 400 nM siRNA. After 24 h incubation, cells were washed three times with PBS, treated with a trypsin-EDTA solution, and suspended in PBS. The fluorescence intensity of the suspended solutions was measured using a BD LSR II flow cytometer (BD Biosciences). The results were expressed as mean and standard deviation obtained from three samples.

Confocal Laser Scanning Microscopic Observation. HuH7-Luc cells were plated on a 35 mm glass-based dish (Iwaki, Tokyo, Japan) at a density of 50 000 cells/well in DMEM supplemented with 10% FBS and incubated for 24 h. The old medium was replaced with fresh medium, and each sample prepared from Cy3-siRNA was applied at 400 nM siRNA. After 24 h treatment with PICs, the transfection medium was removed and then staining with LysoTracker Green (Molecular Probes, Eugene, OR, USA) and Hoechst 33342 (Dojindo, Japan) in the medium was performed. The CLSM imaging was conducted using a LSM 510 (Carl Zeiss, Oberlochen, Germany) equipped with a C-Apochromat 63 \times objective (Carl Zeiss). The LysoTracker Green, Cy3-siRNA, and Hoechst 33342 were excited at 488 nm (Ar laser), 543 nm (He-Ne laser), and 710 nm (MaiTai laser for two-photon imaging), respectively.

The intracellular distribution of Cy3-siRNA was quantitatively evaluated by calculating the co-localization ratio of Cy3-siRNA pixels with LysoTracker Green pixels.^{12,42} The calculation was conducted as follows:

$$\begin{aligned} \text{Co-localization ratio (\%)} &= 100 \\ &\times \frac{\text{number of yellow pixels}}{\text{number of yellow and red pixels}} \end{aligned}$$

The results are expressed as mean and standard deviation obtained from 20 cells.

RNA Recovery from Cultured and Subcutaneous OS-RC-2. Endogenous gene silencing efficiency of SMAs was evaluated using a human renal cell carcinoma, OS-RC-2 (RIKEN Bioresource Center, Tsukuba, Japan). For *in vitro* experiments, the cells were seeded onto a 12-well plate at a cell density of 125 000 cells/well in RPMI-1640 containing 10% FBS. After 24 h incubation, the medium was exchanged, and SMAs containing siVEGF or siSCR

were added at 200 nM siRNA. After 48 h incubation, the cells were lysed in 1 mL of Isogen (Nippon Gene, Tokyo, Japan), followed by RNA extraction by a conventional method with chloroform and 2-propanol. For *in vivo* experiments, Balb/c nude mice (male, 6-weeks-old) were subcutaneously inoculated with OS-RC-2 cells (10^7 cells/mouse), and tumors were allowed to grow for 1 week before sample injection. SMAs prepared at 2 μ M siVEGF or siSCR were concentrated to 10 μ M siRNA using a Vivaspin column (Sartorius Stedim Biotech, Bohemia, NY, USA) and then injected *via* the tail vein two times at days 1 and 2 (25 μ g of siRNA in 200 μ L per injection). At day 3, each tumor was excised and lysed in 0.5 mL of Isogen with sonication, followed by RNA extraction.

Real-Time RT-PCR. After RNA extraction, the RNA concentration in each sample was adjusted to ~ 20 μ g/mL. Genomic DNA elimination and cDNA synthesis were performed using a ReverTra Ace qPCR RT Master Mix with gDNA Remover (Toyobo, Osaka, Japan) according to the manufacturer's protocol. Real-time RT-PCR was performed using an ABI 7500 Fast real-time RT-PCR system (Applied Biosystems, Foster City, CA, USA) with QuantiTect SYBR Green PCR Master Mix (Qiagen, Valencia, CA, USA). Human actin was used as a housekeeper gene (internal standard), and obtained data were normalized before statistical analysis. VEGF primer (forward: AGTGGTC-CCAGGCTGCAC, reverse: TCCATGAACCTCACCACCTCGT) and actin primer (forward: CCAACCGCGAGAAGATGA, reverse: CCAGAGGCGTACAGGGATAG) used for RT-PCR were obtained from Hokkaido System Science (Hokkaido, Japan). The results were expressed as mean and standard error of the mean from four samples.

Hematological Toxicity Assay. SMAs were intravenously injected into the tail vein of Balb/c mice (male, 7-weeks-old), similar to the *in vivo* gene silencing assay (25 μ g of siRNA in 200 μ L per injection). HEPES buffer (10 mM, pH 7.4) containing 150 mM NaCl was used as a control solution. After 24 h, the mice were anesthetized and their blood was collected from the postcaval vein. The collected blood was analyzed to determine the level of ALT and AST with DRI-CHEM 7000i (Fuji Film, Tokyo, Japan) and the level of RBC, WBC, and hemoglobin with pochH-100iV Diff (Sysmex, Hyogo, Japan) according to the manufacturer's protocol. The results were expressed as mean and standard error of the mean from four samples.

Data Analysis. The experimental data were analyzed by Student's *t*-test. $P < 0.05$ was considered statistically significant.

Conflict of Interest: The authors declare no competing financial interest.

Acknowledgment. This research was financially supported by the Funding Program for World-Leading Innovative R&D on Science and Technology (FIRST) from the Japan Society for the Promotion of Science (JSPS) and also by Izumi Science and Technology Foundation. Part of this work was conducted in the Research Hub for Advanced Nano Characterization, The University of Tokyo, supported by the Ministry of Education, Culture, Sports, Science and Technology (MEXT), Japan. We are grateful to Dr. S. Fukuda (The University of Tokyo) and Mr. H. Hoshi (JEOL Ltd.) for their help with TEM observation.

Supporting Information Available: ^1H NMR spectra of PEG-SS-PAsp(DET) (Figure 1a), PEG-PAsp(DET) (Figure 1b), PAsp(DET) with DP = 92 (Figure 1c), and PAsp(DET) with DP = 225 (Figure 1d). Diameter and ζ -potential of silica-coated siRNA PICs prepared at varying sodium silicate concentrations (Figure 2). Agarose gel electrophoresis of siRNA PICs (Figure 3). Diameter of PEG-SS-PAsp(DET)/silica-coated siRNA PICs prepared at varying concentrations of PEG-SS-PAsp(DET) amine (Figure 4). Size distribution histograms of sPICs and SMAs determined by TEM images and the number statistics of DLS (Figure 5). TEM image of SMAs obtained with JEM-1400 (JEOL Ltd., Tokyo, Japan) (Figure 6). Time-dependent change in size of NPC and NDC in 10 mM HEPES buffer containing 150 mM NaCl (Figure 7). Gene silencing efficiency in A549-Luc and SKOV3-Luc cells (Figure 8). These materials are available free of charge *via* the Internet at <http://pubs.acs.org>.

REFERENCES AND NOTES

- Whitehead, K. A.; Langer, R.; Anderson, D. G. Knocking Down Barriers: Advances in siRNA Delivery. *Nat. Rev. Drug Discovery* **2009**, *8*, 129–138.
- Davidson, B. L.; McCray, P. B. Current Prospects for RNA Interference-Based Therapies. *Nat. Rev. Genet.* **2011**, *12*, 329–340.
- Itaka, K.; Kanayama, N.; Nishiyama, N.; Jang, W.-D.; Yamasaki, Y.; Nakamura, K.; Kawaguchi, H.; Kataoka, K. Supramolecular Nanocarrier of siRNA from PEG-Based Block Cationic Carrying Diamine Side Chain with Distinctive pK_a Directed to Enhance Intracellular Gene Silencing. *J. Am. Chem. Soc.* **2004**, *126*, 13612–13613.
- Schiffelers, R. M.; Ansari, A.; Xu, J.; Zhou, Q.; Tang, Q.; Storm, G.; Molema, G.; Lu, P. Y.; Scaria, P. V.; Woodle, M. C. Cancer siRNA Therapy by Tumor Selective Delivery with Ligand-Targeted Sterically Stabilized Nanoparticle. *Nucleic Acids Res.* **2004**, *32*, e149.
- Mao, S. R.; Neu, M.; Germershaus, O.; Merkel, O.; Sitterberg, J.; Bakowsky, U.; Kissel, T. Influence of Polyethylene Glycol Chain Length on the Physicochemical and Biological Properties of Poly(ethylene imine)-graft-poly(ethylene glycol) Block Copolymer/siRNA Polyplexes. *Bioconjugate Chem.* **2006**, *17*, 1209–1218.
- Heidel, J. D.; Yu, Z. P.; Liu, J. Y. C.; Rele, S. M.; Liang, Y. C.; Zeidan, R. K.; Kornbrust, D. J.; Davis, M. E. Administration in Non-human Primates of Escalating Intravenous Doses of Targeted Nanoparticles Containing Ribonucleotide Reductase Subunit M2 siRNA. *Proc. Natl. Acad. Sci. U. S. A.* **2007**, *104*, 5715–5721.
- Kumar, P.; Wu, H.; McBride, J. L.; Jung, K.-E.; Kim, M. H.; Davidson, B. L.; Lee, S. K.; Shankar, P.; Manjunath, N. Transvascular Delivery of Small Interfering RNA to the Central Nervous System. *Nature* **2007**, *448*, 39–45.
- Kim, S. H.; Jeong, J. H.; Lee, S. H.; Kim, S. W.; Park, T. G. Local and Systemic Delivery of VEGF siRNA Using Polyelectrolyte Complex Micelles for Effective Treatment of Cancer. *J. Controlled Release* **2008**, *129*, 107–116.
- Matsumoto, S.; Christie, R. J.; Nishiyama, N.; Miyata, K.; Ishii, A.; Oba, M.; Koyama, H.; Yamasaki, Y.; Kataoka, K. Environment-Responsive Block Copolymer Micelles with a Disulfide Cross-linked Core for Enhanced siRNA Delivery. *Biomacromolecules* **2009**, *10*, 119–127.
- Schaffert, D.; Troiber, C.; Salcher, E. E.; Frohlich, T.; Martin, I.; Badgujar, N.; Dohmen, C.; Edinger, D.; Klager, R.; Maiwald, G.; *et al.* Solid-phase Synthesis of Sequence-defined T-, i-, and U-shape Polymers for pDNA and siRNA Delivery. *Angew. Chem., Int. Ed.* **2011**, *50*, 8986–8989.
- Sieglwart, D. J.; Whitehead, K. A.; Nuhn, L.; Sahay, G.; Cheng, H.; Jiang, S.; Ma, M.; Lytton-Jean, A.; Vegas, A.; Fenton, P.; *et al.* Combinatorial Synthesis of Chemically Diverse Core-Shell Nanoparticles for Intracellular Delivery. *Proc. Natl. Acad. Sci. U. S. A.* **2011**, *108*, 12996–13001.
- Suma, T.; Miyata, K.; Ishii, T.; Uchida, S.; Uchida, H.; Itaka, K.; Nishiyama, N.; Kataoka, K. Enhanced Stability and Gene Silencing Ability of siRNA-Loaded Polyion Complexes Formulated from Polyaspartamide Derivatives with a Repetitive Array of Amino Groups in the Side Chain. *Biomaterials* **2012**, *33*, 2770–2779.
- Morrissey, D. V.; Lockridge, J. A.; Shaw, L.; Blanchard, K.; Jensen, K.; Breen, W.; Hartsough, K.; Machemer, L.; Radka, S.; Jadhav, V.; *et al.* Potent and Persistent *in Vivo* Anti-HBV Activity of Chemically Modified siRNA. *Nat. Biotechnol.* **2005**, *23*, 1002–1007.
- Nakamura, Y.; Kogure, K.; Futaki, S.; Harashima, H. Octarginine-Modified Multifunctional Envelope-Type Nano Device for siRNA. *J. Controlled Release* **2007**, *119*, 360–367.
- Akinc, A.; Zumbuehl, A.; Goldberg, M.; Leshchiner, E. S.; Busini, V.; Ossain, N.; Bacallado, S. A.; Nguyen, D. N.; Fuller, J.; Alvarez, R.; *et al.* A Combinatorial Library of Lipid-like Materials for Delivery of RNAi Therapeutics. *Nat. Biotechnol.* **2008**, *26*, 561–569.
- Xia, T.; Kovoichich, M.; Liang, M.; Meng, H.; Kabehie, S.; George, S.; Zink, J. I.; Nel, A. E. Polyethyleneimine Coating Enhances the Cellular Uptake of Mesoporous Silica

- Nanoparticles and Allows Safe Delivery of siRNA and DNA Constructs. *ACS Nano* **2009**, *3*, 3273–3286.
17. Chen, A. M.; Zhang, M.; Wel, D. G.; Stueber, D.; Taratula, O.; Minko, T.; He, H. X. Co-delivery of Doxorubicin and Bcl-2 siRNA by Mesoporous Silica Nanoparticle Enhances the Efficacy of Chemotherapy in Multidrug-Resistant Cancer Cells. *Small* **2009**, *5*, 2673–2677.
 18. Kakizawa, Y.; Furukawa, S.; Kataoka, K. Block Copolymer-Coated Calcium Phosphate Nanoparticles Sensing Intracellular Environment for Oligodeoxynucleotide and siRNA Delivery. *J. Controlled Release* **2004**, *97*, 345–356.
 19. Pittella, F.; Zhang, M.; Lee, Y.; Kim, H. J.; Tockary, T.; Osada, K.; Ishii, T.; Miyata, K.; Nishiyama, N.; Kataoka, K. Enhanced Endosomal Escape of siRNA-Incorporating Hybrid Nanoparticles from Calcium Phosphate and PEG-Block Charge-Conversional Polymer for Efficient Gene Knockdown with Negligible Cytotoxicity. *Biomaterials* **2011**, *32*, 3106–3114.
 20. Giljohann, D. A.; Seferos, D. S.; Prigodich, A. E.; Patel, P. C.; Mirkin, C. A. Gene Regulation with Polyvalent siRNA-Nanoparticle Conjugates. *J. Am. Chem. Soc.* **2009**, *131*, 2072–2073.
 21. Lee, J. S.; Gree, J. J.; Love, K. T.; Sunshine, J.; Langer, R.; Anderson, D. G. Gold, Poly(beta-amino ester) Nanoparticles for Small Interfering RNA Delivery. *Nano Lett.* **2009**, *9*, 2402–2406.
 22. Decher, G. Fuzzy Nanoassemblies: Toward Layered Polymeric Multicomposites. *Science* **1997**, *277*, 1232–1237.
 23. Becker, A. L.; Johnston, A. P. R.; Caruso, F. Layer-by-Layer Assembled Capsules and Films for Therapeutic Delivery. *Small* **2010**, *6*, 1836–1852.
 24. Davila-Ibanez, A. B.; Salgueirino, V.; Martinez-Zorzano, V.; Marino-Fernandez, R.; Gracia-Lorenzo, A.; Maceira-Campos, M.; Munoz-Ubeda, M.; Junquera, E.; Aicart, E.; Rivas, J.; et al. Magnetic Silica Nanoparticle Cellular Uptake and Cytotoxicity Regulated by Electrostatic Polyelectrolytes–DNA Loading at Their Surface. *ACS Nano* **2012**, *6*, 747–759.
 25. Elbakry, A.; Zaky, A.; Liebl, R.; Rachel, R.; Goepferich, A.; Breunig, M. Layer-by-Layer Assembled Gold Nanoparticles for siRNA Delivery. *Nano Lett.* **2009**, *9*, 2059–2064.
 26. Guo, S.; Huang, Y.; Jiang, Q.; Sun, Y.; Deng, L.; Liang, Z.; Du, Q.; Xing, J.; Zhao, Y.; Wang, P. C.; et al. Enhanced Gene Delivery and siRNA Silencing by Gold Nanoparticles Coated with Charge-Reversible Polyelectrolyte. *ACS Nano* **2010**, *4*, 5505–5511.
 27. Becker, A. L.; Orloff, N. I.; Folini, M.; Cavalieri, F.; Zelikin, A. N.; Johnston, A. P. R.; Zaffaroni, N.; Caruso, F. Redox-Active Polymer Microcapsules for the Delivery of a Survivin-Specific siRNA in Prostate Cancer Cells. *ACS Nano* **2011**, *5*, 1335–1344.
 28. Coradin, T.; Livage, J. Aqueous Silicates in Biological Sol-Gel Applications: New Perspectives for Old Precursors. *Acc. Chem. Res.* **2007**, *40*, 819–826.
 29. Miyata, K.; Gouda, N.; Takemoto, H.; Oba, M.; Lee, Y.; Koyama, H.; Yamasaki, Y.; Itaka, K.; Nishiyama, N.; Kataoka, K. Enhanced Transfection with Silica-Coated Polyplexes Loading Plasmid DNA. *Biomaterials* **2010**, *31*, 4764–4770.
 30. Kataoka, K.; Harada, A.; Nagasaki, Y. Block Copolymer Micelles for Drug Delivery: Design, Characterization and Biological Significance. *Adv. Drug Delivery Rev.* **2001**, *47*, 113–131.
 31. Miyata, K.; Christie, R. J.; Kataoka, K. Polymeric Micelles for Nano-scale Drug Delivery. *React. Funct. Polym.* **2011**, *71*, 227–234.
 32. Nomoto, T.; Matsumoto, Y.; Miyata, K.; Oba, M.; Fukushima, S.; Nishiyama, N.; Yamasoba, T.; Kataoka, K. *In Situ* Quantitative Monitoring of Polyplexes and Polyplex Micelles in the Blood Circulation Using Intravital Real-Time Confocal Laser Scanning Microscopy. *J. Controlled Release* **2011**, *151*, 104–109.
 33. Takae, S.; Miyata, K.; Oba, M.; Ishii, T.; Nishiyama, N.; Itaka, K.; Yakasaki, Y.; Koyama, H.; Kataoka, K. PEG-Detachable Polyplex Micelles Based on Disulfide-Linked Block Cationomers as Bioresponsive Nonviral Gene Vectors. *J. Am. Chem. Soc.* **2008**, *130*, 6001–6009.
 34. Kim, H. J.; Oba, M.; Pittella, F.; Nomoto, T.; Cabral, H.; Matsumoto, Y.; Miyata, K.; Nishiyama, N.; Kataoka, K. PEG-Detachable Cationic Polyaspartamide Derivatives Bearing Stearoyl Moieties for Systemic siRNA Delivery toward Subcutaneous BxPC3 Pancreatic Tumor. *J. Drug Target.* **2012**, *20*, 33–42.
 35. Walker, G. F.; Fella, C.; Pelisek, J.; Fahrmeir, J.; Boeckle, S.; Ogris, M.; Wagner, E. Toward Synthetic Viruses: Endosomal pH-Triggered Deshielding of Targeted Polyplexes Greatly Enhances Gene Transfer *in Vitro* and *in Vivo*. *Mol. Ther.* **2005**, *11*, 418–425.
 36. Saito, G.; Swanson, J. A.; Lee, K.-D. Drug Delivery Strategy Utilizing Conjugation *via* Reversible Disulfide Linkages: Role and Site of Cellular Reducing Activities. *Adv. Drug Delivery Rev.* **2003**, *55*, 199–215.
 37. Corti, A.; Franzini, M.; Paolicchi, A.; Pompella, A. Gamma-glutamyltransferase of Cancer Cells at the Crossroads of Tumor Progression, Drug Resistance and Drug Targeting. *Anticancer Res.* **2010**, *30*, 1169–1181.
 38. Miyata, K.; Nishiyama, N.; Kataoka, K. Rational Design of Smart Supramolecular Assemblies for Gene Delivery: Chemical Challenges in the Creation of Artificial Viruses. *Chem. Soc. Rev.* **2012**, *41*, 2562–2574.
 39. Kanayama, N.; Fukushima, S.; Nishiyama, N.; Itaka, K.; Jang, W.-D.; Miyata, K.; Yamasaki, Y.; Chung, U.-I.; Kataoka, K. A PEG-Based Biocompatible Block Cationomer with High Buffering Capacity for the Construction of Polyplex Micelles Showing Efficient Gene Transfer toward Primary Cells. *ChemMedChem* **2006**, *1*, 439–444.
 40. Miyata, K.; Oba, M.; Nakanishi, M.; Fukushima, S.; Yamasaki, Y.; Koyama, H.; Nishiyama, N.; Kataoka, K. Polyplexes from Poly(aspartamide) Bearing 1,2-Diaminoethane Side Chains Induce pH-Selective Endosomal Membrane Destabilization with Amplified Transfection and Negligible Cytotoxicity. *J. Am. Chem. Soc.* **2008**, *130*, 16287–16294.
 41. Itaka, K.; Ishii, T.; Hasegawa, Y.; Kataoka, K. Biodegradable Polyamino Acid-Based Polycations as Safe and Effective Gene Carrier Minimizing Cumulative Toxicity. *Biomaterials* **2010**, *31*, 3707–3714.
 42. Uchida, H.; Miyata, K.; Oba, M.; Ishii, T.; Suma, T.; Itaka, K.; Nishiyama, N.; Kataoka, K. Odd-Even Effect of Repeating Aminoethylene Units in the Side Chain of N-Substituted Polyaspartamides on Gene Transfection Profiles. *J. Am. Chem. Soc.* **2011**, *133*, 15524–15532.
 43. Takemoto, H.; Ishii, A.; Miyata, K.; Nakanishi, M.; Oba, M.; Ishii, T.; Yamasaki, Y.; Nishiyama, N.; Kataoka, K. Polyion Complex Stability and Gene Silencing Efficiency with a siRNA-Grafted Polymer Delivery System. *Biomaterials* **2010**, *31*, 8097–8105.
 44. Kim, H. J.; Ishii, A.; Miyata, K.; Lee, Y.; Wu, S.; Oba, M.; Nishiyama, N.; Kataoka, K. Introduction of Stearoyl Moieties into a Biocompatible Cationic Polyaspartamide Derivative, PAsp(DET), with Endosomal Escaping Function for Enhanced siRNA-Mediated Gene Knockdown. *J. Controlled Release* **2010**, *145*, 141–148.
 45. Fleming, B. A. Kinetics of Reaction between Silicic Acid and Amorphous Silica Surface in NaCl Solutions. *J. Colloid Interface Sci.* **1986**, *110*, 40–64.
 46. Han, M.; Bae, Y.; Nishiyama, N.; Miyata, K.; Oba, M.; Kataoka, K. Transfection Study Using Multicellular Tumor Spheroids for Screening Non-viral Polymeric Gene Vectors with Low Cytotoxicity and High Transfection Efficiencies. *J. Controlled Release* **2007**, *121*, 38–48.
 47. Mislick, K. A.; Baldeshwieler, J. D. Evidence for the Role of Proteoglycans in Cation-mediated Gene Transfer. *Proc. Natl. Acad. Sci. U. S. A.* **1996**, *93*, 12349–12354.
 48. He, C.; Hu, Y.; Yin, L.; Tang, C.; Yin, C. Effects of Particle Size and Surface Charge on Cellular Uptake and Biodistribution of Polymeric Nanoparticles. *Biomaterials* **2010**, *31*, 3657–3666.
 49. Ferrara, N. VEGF as a Therapeutic Target in Cancer. *Oncology* **2005**, *69*, 11–16.
 50. Takei, Y.; Kadomatsu, K.; Yuzawa, Y.; Matsuo, S.; Muramatsu, T. A Small Interfering RNA Targeting Vascular Endothelial Growth Factor as Cancer Therapeutics. *Cancer Res.* **2004**, *64*, 3365–3370.

51. Kim, S. H.; Jeong, J. H.; Lee, S. H.; Kim, S. W.; Park, T. G. Local and Systemic Delivery of VEGF siRNA Using Polyelectrolyte Complex Micelles for Effective Treatment of Cancer. *J. Controlled Release* **2008**, *129*, 107–116.
52. Pittella, F.; Miyata, K.; Maeda, Y.; Suma, T.; Watanabe, S.; Chen, Q.; Christie, R. J.; Osada, K.; Nishiyama, N.; Kataoka, K. Pancreatic Cancer Therapy by Systemic Administration of VEGF siRNA Contained in Calcium Phosphate/Charge-Conversional Polymer Hybrid Nanoparticles. *J. Controlled Release* **2012**, *161*, 868–874.
53. Christie, R. J.; Matsumoto, Y.; Miyata, K.; Nomoto, T.; Fukushima, S.; Osada, K.; Halnaut, J.; Pittella, F.; Kim, H. J.; Nishiyama, N.; *et al.* Targeted Polymeric Micelles for siRNA Treatment of Experimental Cancer by Intravenous Injection. *ACS Nano* **2012**, *6*, 5174–5189.

PEGylated Polyplex With Optimized PEG Shielding Enhances Gene Introduction in Lungs by Minimizing Inflammatory Responses

Satoshi Uchida¹, Keiji Itaka¹, Qixian Chen², Kensuke Osada², Takehiko Ishii³, Masa-Aki Shibata⁴, Mariko Harada-Shiba⁵ and Kazunori Kataoka^{1,2}

¹Division of Clinical Biotechnology, Center for Disease Biology and Integrative Medicine, Graduate School of Medicine, The University of Tokyo, Tokyo, Japan; ²Department of Materials Engineering, Graduate School of Engineering, The University of Tokyo, Tokyo, Japan; ³Department of Bioengineering, Graduate School of Engineering, The University of Tokyo, Tokyo, Japan; ⁴Laboratory of Anatomy and Histopathology, Faculty of Health Science, Osaka Health Science University, Osaka, Japan; ⁵Department of Molecular Pharmacology, National Cardiovascular Center Research Institute, Osaka, Japan

Safety is a critical issue in clinical applications of nonviral gene delivery systems. Safe and effective gene introduction into the lungs was previously achieved using polyplexes from poly(ethyleneglycol) (PEG)-block-polycation [PEG-block-PAsp(DET)] and plasmid DNA (pDNA). Although PEGylated polyplexes appeared to be safe, an excess ratio of polycation to pDNA was needed to obtain sufficient transgene expression, which may cause toxicities shortly after gene introduction. In the present study, we investigated the combined use of two polymers, PEG-block-PAsp(DET) (B) and homo PAsp(DET) (H) across a range of mixing ratios to construct polyplexes. Although transgene expressions following *in vitro* transfections increased in parallel with increased proportions of H, polyplexes with B/H = 50/50 formulation produced the highest expression level following *in vivo* intratracheal administration. Higher proportions of H elicited high levels of cytokine induction with significant inflammation as assessed by histopathological examinations. Based on the aggregation behavior of polyplexes in bronchoalveolar lavage fluids (BALFs), we suggested that rapid aggregation of polyplexes in the lung induced acute inflammatory responses, resulting in reduced transgene expression. B/H formulation of polyplex can help to improve gene therapy for the respiratory system because it achieves both effective PEG shielding of polyplexes and functioning of PAsp(DET) polycations to enhance endosomal escape.

Received 3 December 2011; accepted 22 January 2012; advance online publication 14 February 2012. doi:10.1038/mt.2012.20

INTRODUCTION

Nonviral techniques for gene introduction using plasmid DNA (pDNA) have attracted attention for many clinical uses. Although the definition of gene therapy includes genetic modification of

deficient cells, gene introduction using pDNA chiefly involves providing functional proteins and peptides through transgene expressions. The sustained synthesis of proteins and peptides, which enables the synchronization of the kinetics of signaling receptor expression and bioactive factor availability,¹ is a key advantage of its application in many chronic diseases.

Among various gene introduction routes, pDNA-containing nanoparticle inhalation, a direct, noninvasive technique, is a promising practical system that makes target cells more accessible. Gene introduction into the respiratory system has numerous applications for treating severe lung diseases, such as cystic fibrosis, pulmonary hypertension, and lung cancer,² and it can systemically deliver proteins and peptides. However, because immune responses of the respiratory system are particularly sensitive to foreign materials, the safety of the delivery systems is extremely important for successful gene introduction. To realize the promise of gene therapy, it is essential to achieve adequate safety to avoid undesirable responses.

pDNA is generally incorporated into nanoscale formulations by complexing it with cationic lipids or polymers, which provides greater stability and functionality.³⁻⁵ The safety of nanoscale particles (nanotoxicology) has been vigorously investigated in various fields.⁶ Many studies revealed that the toxicity of these particles in target tissues, typically the lungs, are primarily mediated by inflammatory responses that occur after nanoparticle-induced oxidative stress.^{7,8} These responses are sensitive to the physicochemical properties of nanoparticles, including their size, chemical composition, surface structure, solubility, shape, and aggregation.⁹⁻¹¹ For delivery into the lungs, a biodegradable formulation of nanoparticles composed of poly(lactic-co-glycolic acid) significantly lowered the inflammatory responses compared with nonbiodegradable forms, although both had comparable hydrodynamic diameters.¹²

These safety issues motivated us to optimize pDNA-containing particle structure for gene introduction into the lungs. Polyplexes from our original cationic polymer, poly{N'-[N-(2-aminoethyl)-2-aminoethyl]aspartamide} [PAsp(DET)] and pDNA,

Correspondence: Kazunori Kataoka, Department of Materials Engineering, Graduate School of Engineering, The University of Tokyo, 7-3-1 Hongo, Bunkyo-ku, Tokyo 113-0033, Japan. E-mail: kataoka@bmw.t.u-tokyo.ac.jp or Keiji Itaka, Division of Clinical Biotechnology, Center for Disease Biology and Integrative Medicine, Graduate School of Medicine, The University of Tokyo, 7-3-1 Hongo, Bunkyo-ku, Tokyo 113-0033, Japan. E-mail: itaka-ort@umin.net

is promising because they are safe and biocompatible.^{13,14} We have already achieved therapeutic outcomes in monocrotaline-induced pulmonary hypertension animal models using a system based on PAsp(DET).¹⁵ PAsp(DET) possesses high-transfection efficiency because of its pH-selective membrane destabilization and concomitantly enhanced endosomal escape.¹⁶ Furthermore, it is biodegradable under physiological conditions. Because of rapid degradation of PAsp(DET) to nontoxic forms after gene introduction, it does not induce persistent tissue damage and cumulative toxicity, which may perturb cellular homeostasis in a time-dependent manner.¹⁷

However, pDNA polyplexes from cationic polymers inevitably have a high surface positive charge, which causes undesirable responses in the body, such as polyplex aggregation and tissue damage. Poly(ethyleneglycol) (PEG) has often been used to shield polyplexes. Because of its hydrophilic and flexible nature, PEG increases steric stability, prevents nonspecific interactions with surrounding molecules, and eventually reduces toxicity.^{18–23} In our previous studies on *in vivo* administrations including the lungs, we used pDNA polyplexes of a micellar structure surrounded by PEG palisade, that were formed by complexing pDNA with a block copolymer composed of PEG and PAsp(DET) [PEG-block-PAsp(DET)].^{15,24,25} These PEGylated polyplexes achieved safe gene introduction without inducing severe inflammation, leading to the effective treatment of rat pulmonary hypertension model using adrenomedullin-expressing pDNA.¹⁵ However, PEG also tends to reduce transgene expressions by preventing cellular uptake of polyplexes and hampering their intracellular processing.^{26,27} Indeed, to obtain sufficient transgene expressions using the PEGylated polyplexes, we needed higher mixing ratios of cationic polymers to pDNA (N/P ratios) to enhance the expressions. The higher N/P ratios, however, caused some toxicities, especially shortly after gene introduction.

In the present study, we investigated the optimal conditions to break out of the dilemma of PEG, by focusing on the intravital behavior of polyplexes in lung. We used a PEGylation strategy by mixing PEGylated and non-PEGylated forms of polycations in the construction of polyplexes-containing pDNA.²² We found that the optimal combination of two forms, PEG-block-PAsp(DET) (B) and homo PAsp(DET) (H), was effective in achieving high transgene expression in lungs with minimal toxicity, by balancing effective PEG shielding and functions of the polycation. Furthermore, we acquired new insights into the mechanisms that mediate the inflammatory responses induced by polyplexes in the lungs.

RESULTS

In vitro and *in vivo* transfection using polyplexes with B/H formulations

For preparation of polyplexes with B/H formulations, the polymer solutions of PEG-block-PAsp(DET) (B) and homo PAsp(DET) (H) were first mixed at different ratios, and then added to pDNA solutions. We conducted *in vitro* transfections toward mouse embryonic fibroblasts and HuH-7 cells using CpG-depleted pDNA-expressing luciferase (pCpG-ΔLuc); the transgene expression was increased in parallel with increased proportions of H (Figure 1) at an N/P ratio of 8. In contrast, cell viability, evaluated by an MTT assay, was reduced slightly with increased proportions of H.

For *in vivo* administration, the polyplexes-containing luciferase-expressing pDNA were injected intratracheally using a microspray, and the luciferase expression was evaluated after extracting the lung tissue, followed by homogenization to obtain the proteins. Polyplexes with B/H = 50/50 formulation exhibited a significantly higher expression in the lungs compared with polyplexes with B/H = 100/0 and 0/100 formulations (Figure 2). These data were in contrast with the results of *in vitro* transfections (Figure 1). To evaluate the toxic effect of polyplexes, we measured

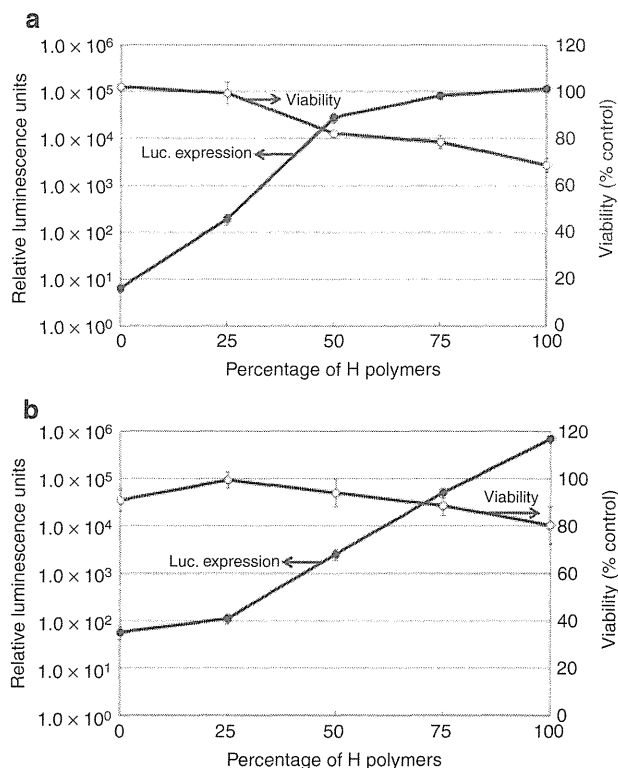


Figure 1 *In vitro* transfection to (a) mouse embryonic fibroblast (MEF) or (b) HuH-7 cells. Luciferase expression (closed circle) and viability (open circle) was measured 48 hours after transfection. The data were expressed as the means ± the standard errors of the mean (SEM) (N = 5).

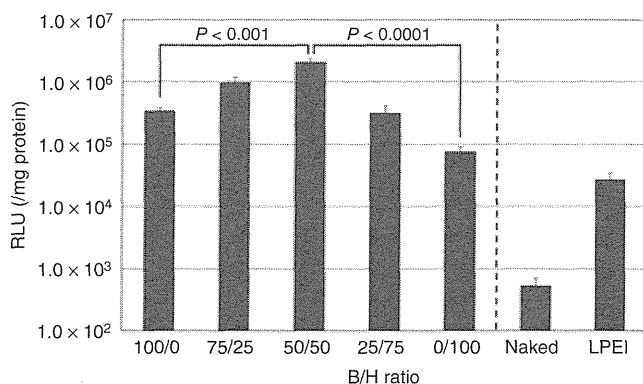


Figure 2 Luciferase expression in lung tissue 48 hours after polyplex administration. The data were expressed as the means ± SEM (N = 5). RLU, relative luciferase units.

the induction of proinflammatory cytokines (interleukin (IL)-6, tumor necrosis factor- α , and IL-10) and cyclooxygenase-2. Polyplexes with B/H = 0/100 formulation induced significantly higher mRNA levels of these inflammation-related molecules compared with other formulations 4 hours after administration (Figure 3). The other PEGylated polyplexes (B/H = 100/0 and 50/50) induced much lower expressions of these molecules than polyplexes with B/H = 0/100 formulation, although the levels of these molecules in the PEGylated groups were slightly higher compared with the control groups that received naked pDNA or buffer.

Furthermore, we evaluated the inflammatory responses to administration of identical amounts of free polymers (B or H) that were used to form the polyplexes of B/H = 100/0 or 0/100 formulations, respectively. The free polymers induced inflammatory responses that were similarly low to those by PEGylated polyplexes (B/H = 100/0 and 50/50) (Figure 3). Thus, it is suggested that the complexation of H polymer with pDNA augmented the inflammatory responses in the lungs compared with the state of free H polymer. In contrast, PEG effectively shielded the polyplexes and reduced the inflammatory responses in the lungs.

After 24 hours of administration, cytokine inductions were similar to the levels observed in the controls (Supplementary Figure S1), suggesting that the inflammation was transient and the PAsp(DET) polycation induced no persistent tissue damage, presumably because of the biodegradability of PAsp(DET).¹⁷ In blood tests conducted 24 hours after administration, there were no

significant changes in the cell counts of white and red blood cells, and the items for evaluations of liver and kidney functions, and C-reactive protein, a sensitive marker for inflammatory responses, remained in an undetectable level (Supplementary Figure S2).

Regulation of inflammatory responses in the lungs by PEG shielding

Histopathological analyses were performed to investigate the mechanisms between transfection capacity and toxicity. An increase in the infiltration of inflammatory cells was observed 4 hours after administration of polyplexes with B/H = 0/100 formulations (Figure 4c). In contrast, following administration of the PEGylated polyplexes (B/H = 100/0 and 50/50), the alveolar structures remained intact without infiltration of inflammatory cells (Figure 4a,b), showing good correlations with the results of proinflammatory cytokine inductions (Figure 3).

To determine the mechanisms underlying the inflammatory responses, we observed the uptake of polyplexes by macrophages. Cy5-labeled pDNAs were introduced into the lungs, followed by immunostaining using an F4/80 antibody for macrophages and Hoechst 33342 for cell nuclei. On obtaining fluorescent microscopic images, we quantified the fluorescence intensities of pDNAs that were colocalized in the macrophages, using an image-analysis software (In Cell Analyzer 1000 Workstation ver.3.5; GE Healthcare UK, Buckinghamshire, UK). Representative microscopic images are shown in Figure 5a–d. As observed in the histograms of the pDNA intensity in each macrophage (Figure 5e),

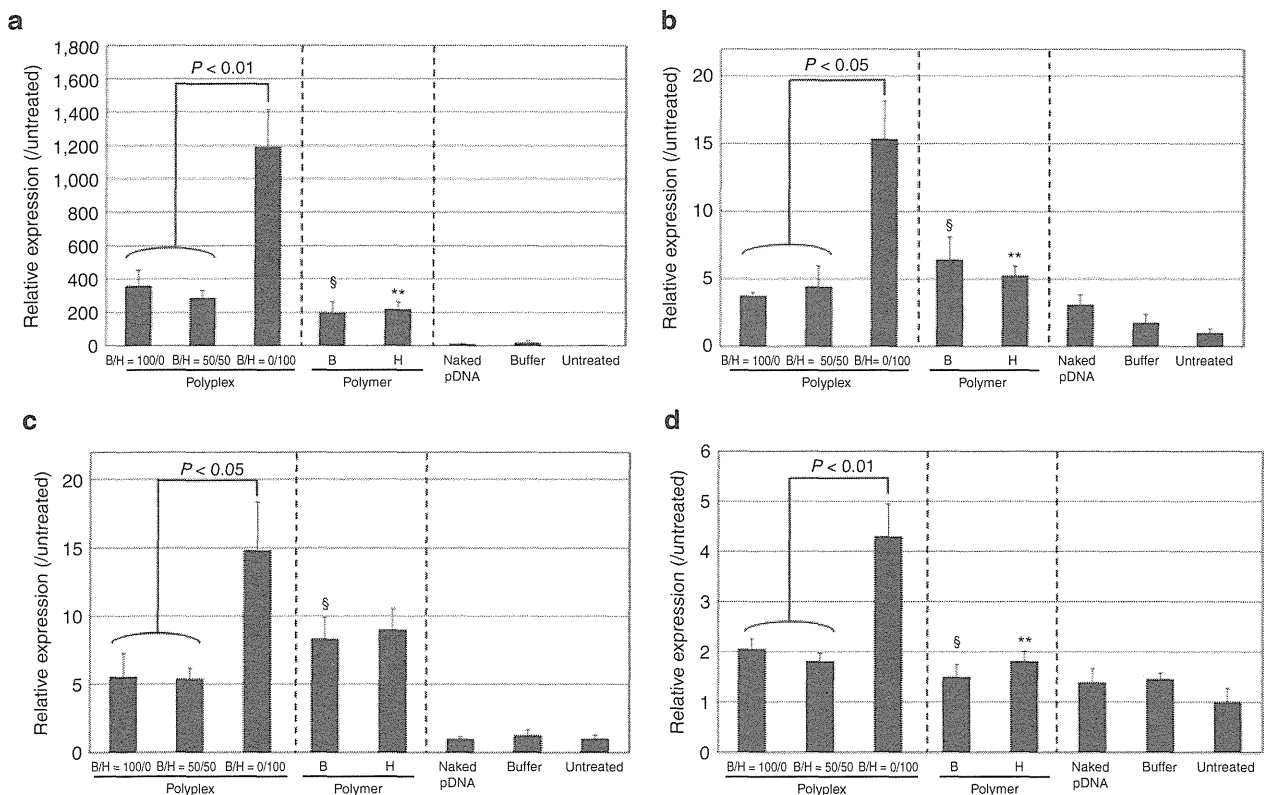


Figure 3 Messenger RNA expression of cytokines (a) interleukin (IL)-6, (b) tumor necrosis factor- α (TNF- α), (c) IL-10, and (d) cyclooxygenase-2 (Cox-2) in lung tissue 4 hours after administration of polyplexes, identical amount of free polymers, plasmid DNAs (pDNAs), or buffer. The data were expressed as the means \pm SEM ($N = 5$). \S Nonsignificance versus polyplexes with B/H = 100/0 formulation, $**P < 0.01$ versus polyplexes with B/H = 0/100 formulation.

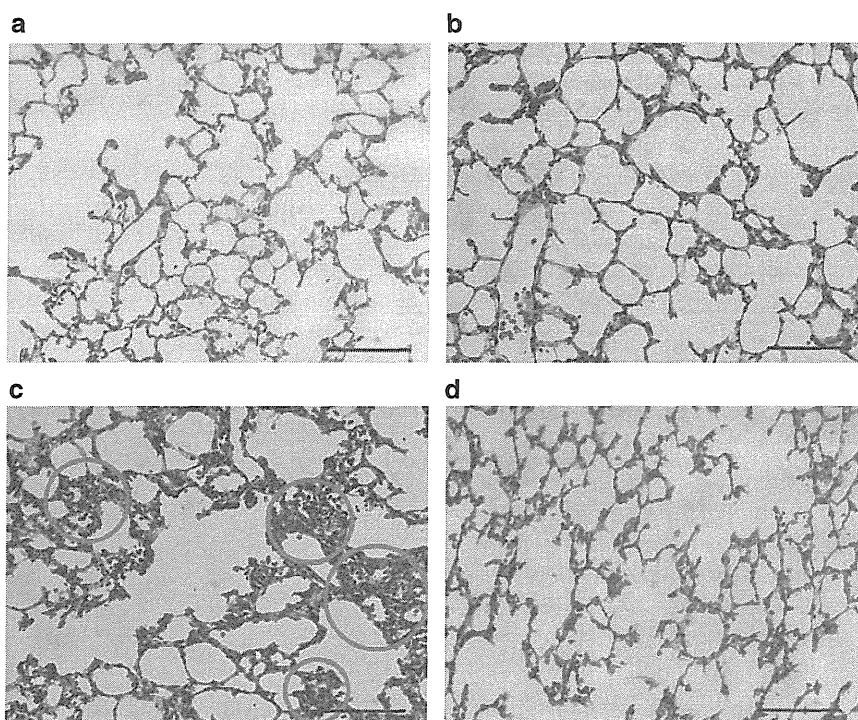


Figure 4 Histological analyses of lung in hematoxylin and eosin stained sections. The images were taken 4 hours after administration of polyplexes with (a) B/H = 100/0, (b) B/H = 50/50, or (c) B/H = 0/100 formulation. (d) Control was not administered polyplexes. Bars = 100 μ m. In (c), representative infiltration of inflammatory cells is marked by red circles.

polyplexes with B/H = 0/100 formulation were taken up by the macrophages to a significantly higher extent compared with the PEGylated polyplexes (B/H = 100/0 and 50/50).

Macrophages are known to effectively ingest large particles ($\geq 500 \mu\text{m}$) by phagocytosis.²⁸ Thus, it is assumed that aggregation of polyplexes in lung tissue may significantly affect the activity of macrophages. Analysis of aggregation of polyplexes under conditions mimicking that observed in the lungs was performed. We observed polyplexes-containing Cy5-labeled pDNAs in the presence of bronchoalveolar lavage fluid (BALF) obtained from mice. Fluorescence microscopy showed a clear contrast between the polyplexes depending on the proportion of H; PEGylated polyplexes (B/H = 100/0 and 50/50) showed uniformly distributed Cy-5 signals during BALF incubation for up to 90 minutes (Figure 6). In contrast, polyplexes with 0/100 formulation showed large spots of Cy-5 signals after 30 minutes of BALF incubation. Thus, it is likely that particle aggregation of B/H = 0/100 formulation was promptly induced under the physiological circumstances in the lungs. Based on the obvious relationship between these findings and the cytokine induction data (Figure 3), we suggest that the aggregation of polyplexes with B/H = 0/100 formulation activated macrophages to rapidly ingest these polyplexes.

Enhancement of transgene expressions in the presence of H polycations

Increased proportions of H enhanced *in vitro* transgene expression (Figure 1). We have already revealed that PAsp(DET) has an excellent capacity of endosomal escape because of acidity-induced membrane destabilization.¹⁶ For the analysis, an enzymatic assay to detect leakage of cytoplasmic enzyme (lactate dehydrogenase)

was done after addition of free polycations to culture cells. However, this experiment has difficulty in detecting the initial changes within several ten minutes after transfection.

In the present study, we used a novel method that allows the evaluation of cell membrane integrity in a highly sensitive manner using a nuclear-binding fluorescence molecule such as YO-PRO1 or ethidium bromide.^{29,30} After transfection using polyplexes from B/H formulations, the cells were treated with YO-PRO1 because YO-PRO1, which was impermeable to the normal cell membrane, can penetrate membranes of cells with perturbed integrity and emit a strong fluorescent signal due to DNA intercalation.³¹ As shown in Figure 7, after 30 minutes of transfection under acidic conditions, polyplexes with B/H = 50/50 formulation destabilized cell membranes to a similar level as polyplexes with B/H = 0/100 formulation, whereas polyplexes with B/H = 100/0 formulation, similar to untreated control, did not destabilize membranes even at pH 5.5. Thus, it can be said that presence of H polycations caused efficient endosomal escape of polyplexes shortly after transfection.

Following *in vivo* administration to the lungs, we evaluated the amount of pDNA that was taken up into the lung tissues by collecting total DNA, followed by quantitative PCR analyses using specific primers for the pDNA. Prior to the extracting lung tissue, extensive bronchoalveolar lavage (BAL) was done to remove pDNAs existing in the extracellular space. Interestingly, 24 hours after introduction of pDNA into the lungs, the amount of pDNA did not show any significant difference among polyplexes formed by different B/H formulations (Supplementary Figure S3). Therefore, it is reasonably assumed that the differences in transgene expressions in the lungs (Figure 2) are not attributable to

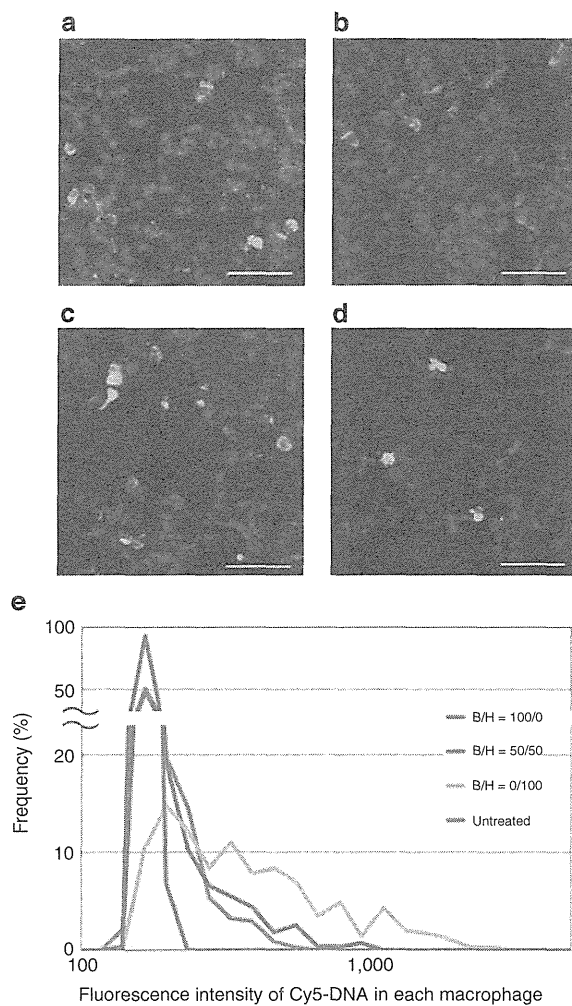


Figure 5 Uptake of polyplexes by macrophages in lung. Fluorescent microscopic images were taken at 4 hours after polyplex administration. The polyplexes were prepared using Cy-5 labeled plasmid DNA (pDNA) (red). The macrophages were immunostained using anti-F4/80 antibodies (green). The cell nuclei were stained with Hoechst 33342 (blue). Representative images of polyplexes with (a) B/H = 100/0, (b) B/H = 50/50, (c) B/H = 0/100 formulations, or (d) control tissue without gene administration. Bars = 50 μ m. (e) Quantification of the amount of pDNA colocalizing in each macrophage. The fluorescence intensities of Cy-5 labeled pDNA in each macrophage were quantified using an image-analyzing software, and displayed as a histogram representing the pDNA intensity in each macrophage.

the uptake of polyplexes into cells, but to the capacities of H polycations to facilitate intracellular processes of endosomal escape, although the direct observation of intracellular behavior of polyplexes was difficult *in vivo*.

DISCUSSION

Inflammation is a key factor in nanoparticle toxicity.^{6,11,32} This is a rapid process that is initially triggered by antioxidant responses within a few hours of exposure of biological tissue to nanoparticles. Thus, it is important to evaluate these responses shortly after the administration of nanoparticles.

In the present study, we determined that PEG shielding of pDNA-containing nanoparticles reduces inflammatory responses

in the lungs. PEGylated polyplexes (B/H = 100/0 and 50/50) effectively alleviated inflammatory responses compared with polyplexes with B/H = 0/100 formulation. Since the administration of free cationic polymers into the lungs did not induce such inflammatory responses, we assume that the cationic nature of polyplexes was not the only cause of these responses. Otherwise, the aggregation behavior was different among polyplexes. Polyplexes with B/H = 0/100 formulation showed rapid aggregation in BALF, whereas PEGylated polyplexes (B/H = 100/0 and 50/50) did not aggregate even after incubation for > 90 minutes (Figure 6). These observations are clearly concordant with the tendency to induce cytokine expression and polyplex uptake by macrophages in the lungs (Figure 3). Thus, it is reasonable to assume that aggregation of polyplex with B/H = 0/100 formulation in lung tissue caused a high uptake of the polyplexes by macrophages, which led to strong inflammatory responses and the decreased transgene expressions in the lung.

Conversely, the presence of PEG on the surface of polyplexes effectively prevents inflammatory responses. Although PEG effectively prevented aggregation, *in vitro* and *in vivo* transgene expressions were compromised by the increase in B polycation. Since pDNA amounts in lung tissues after introduction of polyplexes were not different among the B/H formulations (Supplementary Figure S3), the decrease in the transgene expressions in parallel with the increased ratios of PEG, appeared to be chiefly due to the effects of PEG to hamper the intracellular processes of polyplexes. Membrane destabilization at pH 5.5 was enhanced by the increased amounts of H polycations (Figure 7), suggesting a critical role for H polycations without PEG in facilitating the endosomal escape of polyplexes.³³ As a consequence, polyplexes with B/H = 50/50 formulation showed the highest transgene expression levels with minimal inflammatory responses in the lungs. This formulation successfully took advantage of both effective PEG shielding and the functioning of PAsp(DET) polycations to enhance intracellular processes.

These observations highlight the importance of analyzing intravital behavior of polyplexes from the standpoint of nanotoxicology. Typically presented as transgene expressions in this study, therapeutic outcomes with nanoscale polyplexes can be easily influenced by slight structural modifications, even when no appreciable changes are detected in their *in vitro* physicochemical evaluations. Careful consideration of all processes from polyplex formation to the intravital behavior is required for effective and safe gene and drug delivery systems, especially for administration to the respiratory system.

Based on our originally developed polycation PAsp(DET), which possesses high endosomal escaping capability with minimal toxicity due to its biodegradable nature, we determined the optimal composition of polyplexes for intratracheal administration of pDNA by tuning the mixing ratio of PEG-block-PAsp(DET) (B) and homo PAsp(DET) (H). *In vitro* transgene expressions increased in parallel with increased proportions of H. In contrast, following *in vivo* intratracheal administration into the lungs, polyplexes with B/H = 0/100 formulation significantly induced proinflammatory cytokines and cyclooxygenase-2 expressions, and resulted in histological findings characteristic of inflammation. Using fluorescence microscopy, we found that BALF containing the polyplexes with B/H = 0/100 formulations exhibited rapid aggregate formation. It is thus reasonable to assume that the rapid aggregation of polyplexes with